Mechanically induced cytoskeletal remodeling in trabecular meshwork cells requires TRPV4 - Rho signaling interactions

Running title: Mechanoreciprocity in trabecular meshwork cells

Monika Lakk,[1] David Križaj[1-3]

From the [1]Departments of Ophthalmology & Visual Sciences; [2]Bioengineering; [3]Neurobiology & Anatomy, University of Utah, Salt Lake City, UT

Corresponding author: Monika Lakk, 65 N Mario Capecchi Drive, Bldg. 523, Room S4140 JMEC, Salt Lake City, UT 84132. Email: u6000601@utah.edu

Abbreviations: TM, trabecular meshwork; ROCK, Rho associated protein kinase; FAK, focal adhesion kinase; transient receptor potential vanilloid 4; SACs, stretch activated channels; MLCKs, myosin light chain kinases; MLCPs, MLC phosphatases; IOP, intraocular pressure; ECM, extracellular matrix; αSMA, α-smooth muscle actin; TGFβ, transforming growth factor β; FA, focal adhesion; F-actin, filamentous actin; PTK2, protein tyrosine kinase 2; CICR, Ca^{2+}-induced Ca^{2+} release; CaMKII, Ca^{2+}-calmodulin kinase II, SMCs, smooth muscle cell; PLA2, phospholipase A2, EET, epoxyeicosatrienoic acid; AA, arachidonic acid; hTM, human trabecular meshwork; FBS, fetal bovine serum; Y-27632, *Trans*-4-[(1*R*)-1-Aminoethyl]-*N*-4-pyridinylcyclohexanecarboxamide dihydrochloride; qRT-PCR, quantitative real-time polymerase chain reaction; RIPA, radioimmunoprecipitation assay; PMSF, phenylmethylsulphonyl fluoride; BSA, bovine serum albumin; HRP, horse-radish peroxidase; ir, immunoreactivity.

Acknowledgements

We thank Dr. Mary Beckerle (Huntsman Center, University of Utah) for actin and zyxin reagents and helpful discussions, and Dr. Amy Lin (Moran Eye Center, University of Utah) and Utah Lions Eye Bank for human tissue.

Conflict of Interest

The authors declare that they have no conflicts of interest with the contents of this article.

Author Contributions: Conception and design of research: M.L. and D.K.; conduction of the experiments: M.L.; data analysis: M.L.; interpretation of results: M.L. and D.K.; preparation of figures: M.L. and D.K; drafting of manuscript: M.L. and D.K., editing and revising the manuscript: M.L. and D.K.; approval of the final version of the manuscript: M.L. and D.K.

Keywords: Trabecular meshwork, glaucoma, TRPV4, calcium, integrin, focal adhesion, actin, paxillin, zyxin, cyclic stretch, mechanoreciprocity, glaucoma

Abstract

Intraocular pressure (IOP) is dynamically regulated by the trabecular meshwork (TM), a mechanosensitive tissue that protects the eye from injury through dynamic regulation of aqueous humor outflow from the anterior chamber of the eye. IOP-dependent increases in TM stiffness and contractility drive open angle glaucoma but the mechanotransduction mechanisms that regulate these processes remain poorly understood. We used fluorescence imaging and biochemical analyses to investigate cytoskeletal and focal adhesion remodeling in human TM cells stimulated with cyclic strain. The cells showed enhanced F-actin polymerization, increased number and size of focal adhesions, and activation of the Rho-associated protein kinase (ROCK). Stretch-induced activation of the small GTPase RhoA, and tyrosine phosphorylations of focal adhesion proteins paxillin, focal adhesion kinase (FAK), vinculin and zyxin were time-dependently inhibited by HC-067047, an antagonist of transient receptor potential vanilloid 4 (TRPV4) channels, and the ROCK inhibitor Y-27632. TRPV4 and ROCK activation were required for zyxin translocation and increase in the number/size of focal adhesions in stretched cells. Y-27632 blocked actin polymerization without affecting calcium influx induced by membrane stretch and the TRPV4 agonist GSK1016790A. These results reveal that mechanical tuning of TM cells requires parallel activation of TRPV4, integrins and ROCK, with chronic stress leading to sustained remodeling of the cytoskeleton and focal complexes.

Introduction

The ability of eukaryotic cells to change their cytoskeleton in response to the mechanical environment is critical for a wide range of biological and pathological processes (1, 2). In general, application of tensional forces across the lipid bilayer of nonexcitable cells triggers calcium influx via stretch-activated channels (SACs), with Ca^{2+} signaling mediating activation of myosin light chain kinases (MLCKs), inactivation of MLC phosphatases (MLCPs), disinhibition of caldesmon-dependent myosin ATPases and Rho (Ras homology) GTPases, and activity of nonmuscle myosins (3-5). Calcium-mediated phosphorylation of MLC drives formation of contractile actomyosin units and stress fibers, which exert force on integrins, their cytoskeletal anchoring proteins and modulate downstream pathways such as Rho GTPase-dependent modulation of Rho-associated kinase (ROCK) and LIM kinases (6). SACs, the cytoskeleton and contractility shape the structural and functional plasticity of cells exposed to mechanical stress through focal adhesions (FAs), macromolecular assemblies organized around integrin core that bidirectionally transmit tensile forces between the extracellular matrix (ECM) and the cytoskeleton (6-8). Exertion of mechanical forces across FAs increases the accessibility of the cytosolic integrin tail to actin-binding proteins and induces tyrosine phosphorylations of key FA proteins such as paxillin, focal adhesion kinases (FAKs) and vinculin (7, 9, 10) to augment the cells' resistance to mechanical stress ('mechanoreciprocity'). Ridley and Hall (1992) showed that active RhoA induces formation of stress fibers and FAs but whether and how SACs interact with the Rho pathway and FAs in the presence of forces is not known.

The biomechanical milieu in the vertebrate eye is dominated by intraocular pressure (IOP), which maintains its shape, regulates development of ocular tissues and modulates cellular signaling. IOP is dynamically controlled by the trabecular meshwork (TM), a layered tissue composed of contractile smooth muscle (SM)-like cells populating ECM beams that are anchored to the endothelial cells lining the canal of Schlemm. Mechanical stretch evokes TM contractions (11), thereby increasing the tissue resistance to aqueous humor drainage to elevate IOP (12, 13). At the cellular level, TM cells compensate for pressure-evoked strains with remodeling of cytoskeletal and ECM pathways that inhibit their ability to drain aqueous humor (14). This process malfunctions in hypertensive glaucoma, as TM cells lose the capacity for homeostatic regulation and adopt the myofibroblast phenotype characterized by increased actin polymerization, α–smooth muscle actin (αSMA) expression, deposition of ECM, and transforming growth factor β (TGFβ) release (14-17). Overall, continued exposure to mechanical

stress stiffens the TM and increases its contractility, thereby maintaining IOP in a vicious circle that may result in optic neuropathy (18-20). The remodeling process and IOP elevations in humans and animals with open angle glaucoma can be countered with actin depolymerizers and ROCK inhibitors, which function as IOP-lowering neuroprotective agents in human and animal glaucoma (21, 22). It is therefore of central importance to delineate the molecular mechanisms that drive mechanically induced, Rho-dependent upregulation of TM actin polymerization and contractility.

Here, we tested the hypothesis that force-induced remodeling requires collaboration between transient receptor potential vanilloid isoform 4 (TRPV4), a calcium-permeable polymodal SAC that mediates the responses to strain, swelling, pressure and polyunsaturated fatty acids in TM cells (23-25), and Rho signaling, the actin cytoskeleton and FA pathways. TRPV4 is prominently expressed in mouse and human TM membrane and primary cilia (23, 26) and is often targeted to actin-enriched regions and areas of high strain such as FAs (27-30). Myofibroblast transdifferentiation in smooth muscle, mesenchymal, and endothelial tissues exposed to mechanical stress and/or TGFβ is TRPV4-dependent and bears resemblance to TM remodeling in glaucoma (31-34). In addition, TRPV4 inhibitors protect against fibrosis (33, 34) and lower IOP in a mouse model of glaucoma (23). We found that physiological strain stimuli promote actin polymerization, phosphorylation and/or translocation of key FA-anchoring proteins through a process that requires coordinated activation TRPV4-mediated Ca^{2+} entry and Rho signaling. These findings establish a novel molecular framework that accounts for increased TM stiffness in glaucoma (18), and the efficacy of ROCK/TRPV4 antagonists as IOP-lowering agents in glaucomatous eyes (22, 23).

Materials and Methods

Cell culture

Human trabecular meshwork (hTM cells), isolated from the juxtacanalicular and corneoscleral regions of the human eye (ScienCell Research Laboratories, Carlsbad, CA, USA) were cultured in Trabecular Meshwork Cell Medium (ScienCell Research Laboratories, Carlsbad, CA, USA) supplemented with 2% fetal bovine serum (FBS), 100 units/ml penicillin, 100 μg/ml streptomycin, at 37 ^{o}C and pH 7.4. In accordance with consensus characterization recommendations (23, 24, 35), the phenotype was periodically validated by profiling for markers

MYOC, TIMP3, AQP1, MGP, ACTA2 (α-smooth muscle actin, αSMA) (Supplementary Figure 6A) and DEX-induced upregulation of myocilin protein (Supplementary Figure 6B & C). The morphology, TRPV4 activation and stretch-induced phosphorylation of FAK and zyxin in hTM cells were virtually indistinguishable from cells dissected from nonglaucomatous donor eyes (56 year old, male and 62 year old, female) (23, 24, 35; Supplementary Figure 7). Human tissues were used in concordance with the tenets of the WMA Declaration of Helsinki and the Department of Health and Human Services Belmont Report. Preliminary accounts of this work were published in abstract form (36, 37).

Reagents

The TRPV4 agonist GSK1016790A (GSK101) and antagonist HC-067047 (HC-06) were purchased from Sigma (St. Louis, MO, USA). GSK101 (1 mM), Y-27632 (20 mM) and HC-06 (20 mM) DMSO stocks were diluted in extracellular saline, with the final drug concentrations not exceeding 0.1%. The ROCK1/2 inhibitor *Trans*-4-[(1*R*)-1-Aminoethyl]-*N*-4-pyridinylcyclohexanecarboxamide dihydrochloride (Y-27632) was obtained from Cayman Chemical (Ann Arbor, MI, USA) and the calcium indicator Fura-2 AM from Life Technologies (Carlsbad, CA, USA). Salts were purchased from Sigma (St. Louis, MO, USA) or VWR (Radnor, PA, USA).

Reverse Transcription and Polymerase Chain Reaction (PCR)

Total RNA was isolated using Arcturus PicoPure RNA Isolation Kit according to the manufacturer instructions (Applied Biosystems, Foster City, CA, USA). One microgram of total RNA was used for reverse transcription. First-strand cDNA synthesis and PCR amplification of cDNA were performed using qScript^{TM} XLT cDNA Supermix (Quanta Biosciences. Beverly, MA, USA). The RT-PCR products were run on 2% agarose gels and visualized by ethidium bromide staining, along with 100-bp DNA ladder (Thermo Fisher Scientific, Waltham, MA, USA).

Quantitative Real-Time Polymerase Chain Reaction (Q-RT-PCR)

SYBRGreen based real-time PCR was performed using Apex qPCR GREEN Master Mix (Genesee Scientific, San Diego, CA, USA). The experiments were performed as triplicates of at

least three independent experiments and are expressed as a ~fold change compared to the control. The C_T method ($\Delta\Delta C_T$) was used to measure relative gene expression where the ~fold enrichment was calculated as: $2^{-[\Delta CT\ (sample)\ -\Delta CT\ (calibrator)]}$ after normalization. GAPDH and β-tubulin were utilized as endogenous controls to normalize the fluorescence. The primer sequences are listed in Table 1.

Western Blots

Cells were lysed on ice using a radioimmunoprecipitation assay (RIPA) lysis buffer system (Santa Cruz Biotechnology, Dallas, TX, USA) containing PMSF, sodium-orthovanadate and protease inhibitor cocktail (Santa Cruz Biotechnology, Dallas, TX, USA) to avoid degrading processes. An equal amount of protein (20-25 μg) was loaded in 10 or 12 % SDS-polyacrylamide gels. Samples were transferred to polyvinylidene difluoride (PVDF) membranes for 1h at 300 mA. The non-specific binding sites were blocked with 5% non-fat milk and 1% bovine serum albumin (BSA) and incubated overnight at 4 ºC with primary antibodies. Primary antibodies and their specifications are listed in Table 2. The binding of the primary antibodies was quantitated with anti-mouse (1:2000, Life Technologies, Carlsbad, CA, USA) or anti-rabbit (1:3000, Cell Signaling, Danvers, MA, USA) horseradish peroxidase (HRP)-conjugated secondary antibodies. HRP conjugated anti-rabbit-GAPDH (1:10.000, Abcam, Cambridge, MA, USA) antibody was used as loading control. The blotted proteins were developed using an enhanced chemiluminescence kit (Thermo Fisher Scientific, Waltham, MA, USA).

Rho Activity Assay

GTPase activity was assessed with the Active Rho Detection Kit (Cell Signaling, Danvers, MA, USA) according to the manufacturer's instructions. Briefly, the assay takes advantage of GTP-bound Rho (active form) binding to the Rhotekin-RBD fusion protein, expressed as a GST-fusion protein in *E. coli*. The protein shows selectivity for GTP-bound as opposed to “inactive” GDP-bound RhoA, RhoB and RhoC isoforms and precipitates active Rho proteins on glutathione resin. The level of activation was quantified with Western blots (the Rho antibody obtained from Cell Signaling was used at 1:500).

Immunofluorescence

Apoptosis assay: cells were pre-incubated with SRB-VAD-FMK, a cell permeable fluorogenic caspase probe (1:250, AAT Bioquest, Sunnyvale, CA, USA) at 37 ºC, 5% CO_2 for 1 hour before fixation. Cells were fixed with 4% paraformaldehyde for 10 min and blocked in PBS (5% FBS and 0.3% Triton X-100) for 20 min (124, 127). Alexa Fluor 488 phalloidin (Life Technologies, Carlsbad, CA, USA) was utilized for F-actin staining (1:1000 for 1 hr). Primary antibodies (Table 2) were diluted in PBS (2% BSA and 0.2% Triton X-100) and incubated overnight at 4°C. After rinsing, the cells were incubated for 1 hour at RT with goat anti-mouse and goat anti-rabbit IgG (H + L) secondary antibodies conjugated to fluorophores (Alexa Fluor 488 nm, 568 nm and/or 594 nm; 1:500; Life Technologies, Carlsbad, CA, USA). Unbound antibodies were rinsed and conjugated fluorophores protected with Fluoromount-G (Southern Biotech, Birmingham, AL, USA) prior to mounting coverslips. Images were acquired on a confocal microscope (Olympus FX1200) at 1024 x 1024 pixels with a 20X water superobjective (1.00 N.A.; field size: 158.565 x 158.565 µm; 0.155 µm/pixel; sampling speed: 10.0 us/pixel; 12 bits/pixel).

Immunofluorescence analysis

Images were acquired using identical parameters (HV, gain, offset) resulting very similar signal noise across datasets. ImageJ was used to extract and quantify the mean intensities of immunoreactive signals.

Particle counting and colocalization: Particle analysis was performed using ImageJ, with ~40-50 cells per slide averaged across at least 3 independent experiments. Color images were converted to black and white using *Binary→Convert to mask* with white background and automatic threshold level. Immunoreactive puncta (number/cell area) with the segmented area were counted with the *Analyze particles* plugin. Minimum (3 pixel^2) and maximum (50-70 pixel^2) pixel area sizes were defined to exclude areas outside of the ROI, calculate the particle number/cell area and determine the relative particulum numbers. Individual particulum sizes for each cell were averaged and normalized. The particulum size was not maximized for p-zyxin analysis in order to capture the particles that translocated along the stress fibers. Colocalization (i.e., overlap of fluorescence for each pixel) was determined for images (Color 1/protein 1 and Color 2/protein 2) that were converted to black/white (*Binary→Convert to mask*). To visualize only the colocalized particles, a window was generated with *Process→Image calculator* and the

multiply panel. Colocalized pixels were counted following the subtraction of noise as described above. Minimum pixel size (2 pixel^2) and maximum area (50-70 pixel^2) were determined to exclude objects outside of the area of interest. % colocalization corresponds to the overlap in particulum number/cell area for Colors 1 and 2.

Strain application

Strain (substrate deformation) was applied as described (23, 38), using the computer-controlled vacuum-operated Flex 5000 Jr. Tension System (Flexcell International Corporation, Burlington, NC, USA). Cells were plated onto collagen-coated silicon membranes and exposed to cyclic biaxial stretch (6% elongation, 0.5 Hz) for indicated times (1, 3, 5 or 7 hours). Control cells were cultured under the same conditions, but no mechanical force was applied. Y-27632 (10 μM), GSK101 (5 nM) or the HC-06 (1 μM) were added to culture media 30 min prior to stretching. Stretch-induced Ca^{2+} influx was studied in cells loaded with Fura-2-AM (5-10 μM) for 60 minutes and stimulated with biaxial stretch (10% elongation, 1 Hz, 15' or 30'). The cells were imaged with an upright Nikon E600FN microscope and a 40x (0.8 N.A. water) objective. 340/380 nm excitation was provided by a Xenon lamp within a Lambda DG4 (Sutter Instruments, Novato, CA, USA) wavelength switcher.

Calcium imaging

Pharmacological experiments were conducted in fast-flow chambers (Warner Instruments, Hamden, CT, USA) on cells loaded with 5-10 μM Fura-2-AM (K_d at RT = 225 nM) for 45 min (23, 128). The saline (pH 7.4) contained (in mM): 98.5 NaCl, 5 KCl, 3 $MgCl_2$, 2 $CaCl_2$, 10 HEPES, 10 D-glucose, 93 mannitol. TRPV4 and Rho reagents were placed into reservoirs connected to a gravity-fed perfusion system (Warner Instruments, Hamden, CT, USA). Epifluorescence imaging was performed on inverted Nikon microscopes using 40x (1.3 N.A., oil or 0.80 N.A., water) objectives, with excitation for 340 nm and 380 nm filters (Semrock, Lake Forest, IL, USA) delivered by a 150W Xenon arc lamp (DG4, Sutter Instruments) and 2 x 2 binning. Fluorescence emission was high pass-filtered at 510 nm and captured with cooled EMCCD cameras (Photometrics, Tuscon, AZ, USA). ΔR/R (peak F_{340}/F_{380} ratio – baseline/baseline) was used to quantify the amplitude of Ca^{2+} signals which were acquired and analyzed using NIS Elements 3.22 software.

Plasmid Constructs and Live Actin Imaging

TM cells were transfected with mApple:actin (0.5 μg/ul) or mCherry:actin (0.5 μg/μl) DNA constructs using Lipofectamine (Invitrogen, Carlsbad, CA, USA). Lipofectamine and DNA were diluted separately in Opti-MEM medium; after a quick incubation at RT, the DNA solution was mixed into Lipofectamine solution; the mixture was incubated at RT for about 20 min to obtain the desired N/P ratios. After 24 hour after incubation with the constructs, cells were loaded for 45 min with Fura-2-AM (5-10 μM). TRPV4 and Rho reagents were placed into reservoirs connected to gravity-fed perfusion systems (Warner Instruments, Hamden, CT, USA). *mApple:actin*/*mCherry:actin* and Fura-2 fluorescence were concurrently imaged with a 40x (1.4 N.A. oil) objective (Nikon Ti, Technical Instruments, San Francisco, CA, USA).

Statistical Analysis

Data are presented as means ± SEM. For histochemistry, ≥10 per experiment were acquired for at least 3 independent experiments. For calcium imaging, ~10-20 cells per slide were averaged across ~3-6 slides per experiments and 3 independent experiments. Western blot data includes at least 3 separate experiments. Cell numbers = "n", independent experiments = "N". The statistical comparisons were determined by one-way ANOVA followed by post-hoc Tukey's multiple comparison of means (Origin 8.0, Origin Lab Corporation, Northampton, MA, USA). $P \leq 0.05$ (*), $P \leq 0.01$ (**), $P \leq 0.001$ (***) and $P \leq 0.0001$ (****) values were considered statistically significant.

Results

Stretch-dependent actin stress fiber formation requires TRPV4 activation and Rho signaling

Force-production in non-muscle cells relies on cross-linked actomyosin structures (6, 39). Generally, these are visualized as fluorescently tagged cell-traversing arrays of filamentous actin (F-actin) stress fibers that attach to membrane focal contacts. Physiological levels (6%, 1 hour) of cyclic strain that produce half-maximal $[Ca^{2+}]_{TM}$ responses on the stretch-response curve (23) had no effect on shape or viability of TM cells (Supplementary Fig. 1). Indicating that polymerization of TM F- actin is sensitive to mechanical stress, increased tension was associated with significant increases in stress fiber fluorescence (41.7 ± 4.2%; N = 4; $P < 0.05$) (Fig. 1). The

selective TRPV4 blocker HC-067047 (HC-06; 1 µM) did not affect phalloidin signals in resting cells (97.6 ± 4.8%; N = 4) (Fig. 1A & B) but reversed the stress fiber upregulation induced by stretch (to 103.11 ± 4.45%; N = 4; P < 0.01) (Fig. 1A & B). Stress fiber fluorescence in non-stretched cells was not significantly affected by the ROCK inhibitor Y-27632 (10 µM) (88.52 ± 11.65%; N = 4; Fig. 1A & B), whereas ROCK inhibition suppressed the effect of stretch to 71.57 ± 4.81% (P < 0.01; N = 4; Fig. 1A & B). TM cell survival was unaffected by the exposure to HC-06 or Y-27632 (Supplementary Fig. 1B & C). These observations suggest that *de novo* actin polymerization triggered by mechanical stretch requires activation of TRPV4 and Rho signaling pathways.

Rho/ROCK signaling pathway is downstream from TRPV4

To gain insight into TRPV4 and ROCK mechanisms that underlie stress fiber formation, we conducted ratiometric calcium imaging in the presence of the TRPV4 agonist GSK101 (5 nM) and/or Rho/TRPV4 inhibitors (Fig. 2A-D). GSK101 elevated ΔR/R to 0.81 ± 0.04 ± 0.27 (n = 164; P < 0.0001; Fig. 2A & D), whereas ROCK inhibition had no significant effect on basal $[Ca^{2+}]_i$ (0.13 ± 0.01; n = 66; Fig. 2B & D), the amplitude of GSK101-induced calcium signals (0.82 ± 0.06; n = 52; Fig. 2C & D) or F-actin signals (Fig. 1B). GSK101 similarly facilitated the formation of actin stress fibers in cells transfected with *mCherry:actin* or *mApple:actin* (n = 4; Fig. 2Ai-iii). Y-27632 alone non-significantly (Supplementary Fig. 2A) reduced resting stress fiber fluorescence (n = 4; Fig. 2Bi-iii), while concurrent administration of Y-27632 inhibited the activating effect of 5 nM GSK101, resulting in decreased number of stress fibers (n = 4; Fig. 2Ci-iii). In contrast to stretch-induced stress fiber sensitivity to ROCK (Fig. 1), $[Ca^{2+}]_i$ elevations induced by 15 or 30 min cyclic stretch (to 0.23 ± 0.02 and 0.22 ± 0.02, respectively; n = 30, N = 4; P < 0.0001) were unaffected by Y-27632 (Fig. 2E & Supplementary Fig. 2B), suggesting that Rho-dependent formation of actin stress fibers is downstream from TRPV4. The sensitivity of stretch- and GSK101-induced stress fiber formation to Y-27632 confirms that ROCK is required for actin polymerization driven by both mechanical and chemical inputs.

The small GTPase RhoA is activated by stretch in a TRPV4-dependent manner

We next investigated the stretch-dependence of the small GTPase RhoA, an early responder to tension applied to integrins (40, 41) and a prominent regulator of the TM cytoskeleton (19). One

hour of stretch resulted in three-fold increase in RhoA mRNA (3.00 ± 0.72; N = 4; P < 0.05) which was downregulated at longer stretch durations (Fig. 3A). This effect was associated with significant increases in levels of the active (GTP-bound) Rho protein (1.56 ± 0.12; N = 3; P < 0.05) whereas GDP-bound protein levels remained unchanged (Fig. 3B & C). HC-06, but not Y-27632, significantly suppressed stretch-induced upregulation of the active Rho protein (0.99 ± 0.05; P < 0.05; Fig. 3B & C). Hence, tensile strain modulates RhoA transcription and activation in a TRPV4 -dependent manner, but without feedback from ROCK.

Stretch-induced phosphorylation and targeting of Focal Adhesion Kinase (FAK) requires time-dependent TRPV4 activation and Rho signaling

Stress fibers generate force by pulling on adhesion sites, which impose stress on the cytoskeleton via adapter and anchor proteins (10, 42). Mechanical strain facilitates formation of FAs, which are enriched in phosphotyrosinated proteins (43). A particularly important anchoring protein, activated by mechanically induced integrin clustering (44, 45), is the Focal Adhesion Kinase (FAK). Phosphorylation of FAK was reported to subserves TM stiffness on rigid substrates (46), regulate phagocytosis (47), myocilin-dependent integrin β1 signal transduction (48) but also maintain the structural stability of actin (49). The Protein Tyrosine Kinase 2 (PTK2) gene that encodes FAK was modestly (1.57 ± 0.12-fold) but significantly (N = 3; P < 0.05) upregulated following 3 hrs strain stimulation and was unaffected at 5 and 7-hour time points (Fig. 4A). We tested whether stretch affects FAK expression and activation by labeling the protein for autophosphorylation at Tyr397 (44, 50). Total FAK protein levels remained constant, but phosphorylation was augmented at 1 and 3 hours to 2.11 ± 0.07; 2.28 ± 0.16 - fold, respectively (N = 3-5; P < 0.01; Fig. 4B). At 1 hour, Y-27632 suppressed phosphorylation (to 0.88 ± 0.14; N = 3; P < 0.05) whereas HC-06 had no effect (at 1.87 ± 0.20; N = 3). At 3-hours stretch, FAK phosphorylation was inhibited by both TRPV4 and ROCK antagonists (Fig. 4C & D). These data suggest that use-dependent formation of FAK-containing focal complexes in the presence of mechanical stress requires time-dependent ROCK and TRPV4 signaling.

Transient paxillin phosphorylation is an early step in the TM stretch response

FAK shares the submembrane focal space with paxillin, a 64.5 kDa multidomain scaffolding protein that integrates mechanical cues from the ECM with the integrins (51, 52). Stretch does

not affect the levels of paxillin mRNA and total protein at any time point (N = 3; Fig. 5A, black bars in B & C). However, Western blots showed a striking elevation in activated paxillin (Tyr118 phosphorylation) at 1 hour of stretch, with 2.54 ± 0.27 (N = 3; P < 0.01) increase (red bars in Fig. 5B). The effect of stretch was blocked by HC-06 (1 µM; 1.18 ± 0.08; N = 3; P < 0.05) and the calcium chelator BAPTA-AM (100 µM; 0.63 ± 0.06; N = 3; P < 0.01), but not by Y-27632 (10 µM; N = 3; P = 0.216) (Fig. 5Di-ii). These data implicate paxillin activation in early, stretch-and time -dependent TM remodeling that requires TRPV4 and Ca^{2+}. Consistent with this, 1 hour stretch caused a remarkable increase in the number of p-paxillin-immunoreactive (ir) (Tyr31-phosphorylated) puncta (to 1.69 ± 0.11; N = 3; P < 0.05 (Fig. 5E & F and Supplementary Fig. 3) without affecting the number of vinculin-ir puncta (Fig. 5F and Supplementary Fig. 3). However, stretch significantly enhanced the extent of vinculin and p-paxillin colocalizations (from 0.20 ± 0.04 to 0.45 ± 0.10 and from 0.51 ± 0.10 to 0.69 ± 0.07, respectively; N = 3; P < 0.05) in a TRPV4-, BAPTA- and ROCK-dependent manner (Fig. 5G and Supplementary Fig. 3).

Stretch promotes colocalization between vinculin and pFAK

Paxillin is recruited to the actin network by the N-terminal domain of vinculin, a key FA protein that regulates integrin and anchor protein dynamics that are required for the enlargement of the focal complex (53). The recruitment of vinculin to stress fiber-anchored FAs was force-dependent (Fig. 6C, F & G). While mRNA and total vinculin protein expression remained unaffected by stretch (Fig. 6A & B), increased colocalization between vinculin and pFAK was observed at 1 and 3 hours (from 46 ± 3% to 58 ± 3% in 1 hr samples and from 57 ± 2% to 71 ± 2% in 3 hr samples; P < 0.05; N = 3) (Fig. 6F & G). This effect was sensitive to Y-27632 at 1 hour (to 39.39 ± 5.04%; P < 0.05; N = 3) and HC-06 at 3 hours (54 ± 4%; P < 0.05; N = 3; Fig. 6F & G). In resting cells, vinculin colocalized with pFAK at the edges of stress fibers (Fig. 6C), with the number of pFAK-ir FA clusters increasing at 1 and 3 hour stretch (by 65.79 ± 20.22% and 34.54 ± 1.01%; P < 0.01 and 0.001, respectively; N = 3; Fig. 6D & E). The increase in immunoreactive puncta was associated with a modest but significant increase in pFAK - vinculin colocalization (from 76.03 ± 2.36% to 85.44 ± 1.25% and from 74.12 ± 1.12 to 86.65 ± 3.1%, respectively; P < 0.05; N = 3) (Fig. 6F & G). Y-27632, but not HC-06, inhibited pFAK upregulation and its interaction with vinculin at 1 hour, whereas HC-06 and Y-27632 both

suppressed the effect after 3 hours of stretch (Fig. 6C-G). These findings confirm the Rho-dependence of FAK activation (54) and suggest that TRPV4-dependent regulation of FAK-vinculin-containing FAs involves time-dependent Rho signaling.

Stretch also induced increases in vinculin-ir (1.27 ± 0.05; $P < 0.01$; N = 3) and FA size that were antagonized by ROCK and TRPV4 blockers to 1.01 ± 0.03 and 1.05 ± 0.08, respectively ($P < 0.05$; N = 3) (Fig. 7A, B and Supplementary Fig. 4A). We tested for stretch-dependence of vinculin activation by labeling for Tyr1065, which is important for force generation (55). A significant increase in activated vinculin (1.78 ± 0.25; $P < 0.05$; N = 3) was observed following 1 hour of stretch, an effect that was suppressed by Y-27632 (0.75 ± 0.1; $P < 0.05$; N = 3) and HC-06 (0.99 ± 0.25; $P < 0.05$; N = 3) (Fig. 7C, D and Supplementary Fig. 4B). Thus, stretch-induced vinculin activation requires Rho and TRPV4 signaling.

Stretch-induced translocation of zyxin from FAs to polymerized actin requires TRPV4 and calcium

The FA protein zyxin mediates force-dependent interactions between actin regulatory proteins and actin (56, 57) and is sensitive to TGFβ2, a glaucoma-promoting cytokine known to drive TM actin polymerization (58, 59). Assessment of zyxin mRNA and protein levels after 1 - 7 hours exposure to cyclic strain showed significant upregulation in transcription following 1 hour (2.35 ± 0.19-fold) and 5 hours (2.43 ± 0.22-fold) of stretch (N = 3-4; $P < 0.01$; Fig. 8A & B), whereas total zyxin protein levels were unaffected for up to 7 hours (2.55 ± 0.16; N = 3; $P < 0.05$) (Fig. 8B & C). As with other FA adhesome components (Fig. 4 & 5), stretch augmented zyxin phosphorylation (at S142/143) by 2.45 ± 0.48 and 2.69 ± 0.48- fold following 1- and 3-hour stretch, respectively (N = 3-4; $P < 0.05$ and 0.01; Fig. 8B & C). Zyxin phosphorylation at 1 hour was unaffected by Y-27632, HC-06 or BAPTA (Fig. 8C, D & Ei-ii), whereas TRPV4 and ROCK blockade significantly reduced the levels of phosphorylated-zyxin at 3 hours stretch (1.18 ± 0.31 and 1.32 ± 0.29, respectively; N = 3-4; $P < 0.05$) (Fig. 8C & D). In unstimulated cells, zyxin-ir was largely confined to FA sites whereas stretch induced a remarkable translocation towards actin stress fibers (Fig. 9 and Supplementary Fig. 5), an effect that was sensitive to HC-06 and Y-27632. Zyxin translocation induced by strain was presumably associated with increased cytoskeletal tension and contractility (60-62).

Discussion

This study identifies the molecular mechanism through which physiological strains regulate the architecture and function of trabecular meshwork cells. We employed strains that mirrored *in situ* biomechanical stress on corneoscleral beams and juxtacanalicular lamellae (~10% –20% strain for pressure differentials of ~5 – 15 mm Hg) (63-65), and a stretch cycle (1 Hz) that reflected ocular pulse dynamics (e.g., 66, 67), to discover that cyclic strains induce cytoskeletal and FA remodeling through obligatory activation of TRPV4 channels, Rho signaling, and TRPV4-Rho interactions. Our data suggest that TRPV4 functions as a likely SAC transducer of TM stretch response and a strong candidate for driving myofibroblast transdifferentiation and cell stiffening associated with stretch- and IOP-dependent increases in F-actin, tyrosine phosphorylation, αSMA & Rho-ROCK signaling and TGFβ release (15, 18, 66, 68-73). Given that strain represents a principal aspect of IOP-generated mechanical force that shapes trabecular outflow (65) whereas cytoskeletal remodeling constitutes the central aspect of glaucomatous TM remodeling (19), elucidation of TM mechanotransduction and Rho signaling pathways brings insight into the biology of the ocular outflow system and identifies pathways that can be targeted to reverse cytoskeletal impairments in glaucoma.

Our results establish a mechanistic framework for how TRPV4 antagonists, actin disruptors and ROCK inhibitors suppress TM stiffness, ECM release and IOP in hypertensive eyes (21-23, 73, 74-77) by adding two important insights: First, Rho signals are downstream from TRPV4, with TRPV4 mechanotransduction; Second, ROCK activation is both necessary and sufficient for increased F-actin polymerization induced by cyclic mechanical strain. By implicating the FA 'adhesome' (6) in increased contractility in mechanically stressed TM cells (11, 72), our data provide the molecular context for mechanotransduction-dependent regulation of the outflow pathway. The obliteration of stretch-evoked increases in stress fiber fluorescence by the cell-permeable pyridine derivative Y-27632 (Fig. 1 & 2) is consistent with ROCK functioning as the master regulator of actin polymerization, contractility and remodeling in mechanically stressed TM (22, 74). Rao's group found that stretch elevates the TM levels of activated RhoA, phosphorylated paxillin and MLCK through aberrant Rho/ROCK activation. Here, we identify TRPV4 as the mechanochannel that is required for dynamic remodeling of F-actin and ROCK-dependent upregulation of integrin-ECM contacts. TRPV4 and ROCK blockers reduced the number and size of activated FAs, and suppressed colocalization between key

components of the FA complex (p-paxillin and vinculin, pFAK and vinculin; Fig. 5, 6 & 7), indicating that synergistic contribution of the SAC and ROCK to strain-dependent formation, maturation and maintenance of FAs that reinforces TM cytoarchitecture in the presence of chronic strains.

Membrane stretch promotes F-actin and αSMA expression, MLCK phosphorylation and biosynthesis of ECM that inhibit aqueous outflow (19, 72, 78). Indicating that TRPV4 functions as the SAC that mediates stretch-induced cytoskeletal stiffening, GSK101 mirrored the effect of stretch on stress fiber formation whereas HC-06 blocks stretch-induced F-actin upregulation. ROCK inhibition downregulated pMLCK and αSMA and suppressed F-actin polymerization (66, 72, 75) whereas Y-27632 had no effect on TRPV4-induced $[Ca^{2+}]_i$ signals (Fig. 2). This indicates that ROCK signaling is downstream from TRPV4-mediated Ca^{2+} influx and rules out a major role for cytosolic or membrane Rho signaling (79) in TRPV4 channel gating, translocation and/or expression. Consistent with this conclusion, the effects of cyclic stretch on cytoskeletal remodeling and myofibroblast transformation can be substituted by either constitutive activation of the Rho pathway (72, 80, 81) or TRPV4 overactivation (31, 34, 82). To the best of our knowledge, our study is among the first to systematically examine the convergence of the two pathways at the level of multiple constituents of the tensile transduction mechanism.

In general, SAC gating is influenced by the properties of the lipid bilayer and by channel interactions with the cytoskeleton and the ECM. The obligatory involvement of TRPV4 in force-induced stress fiber formation, FA reinforcement and fibrosis accords with its functions as a transducer of pressure (24, 83), ECM stiffness (84), cell swelling (38, 85-87), shear stress (88, 89), and its roles in gene expression, integrin signaling (90), tensile activation of vinculin (91) and fibrotic remodeling (34). In contrast to Piezo1 and TREK1 channels which are directly activated by pressure/stretch/indentation (92, 93), the biophysical mechanism that activates TRPV4 channels in the presence of strain is not understood (38, 85, 94-96, 83, 84, 97, 98). Interestingly, β1 integrins activate TRPV4 (5, 30, 90), are expressed in human and mouse TM (99, 100, 101), interact with ROCK (79), and contribute to IOP regulation and glaucoma (102, 103) whereas pretreatment with FAK or β1 integrin inhibitors suppressed sensitization of TRPV4 channels by mechanical stressors (89). Another potential clue is arachidonic acid, which is released by mechanically stimulated TM cells and activates TRPV4 (98, 99). This

polyunsaturated ω6 fatty acid might therefore enhance TM sensitivity to weak hydrodynamic loading (23, 96).

Our data identify TRPV4 -mechanotransduction as a venue for Ca^{2+} influx that is necessary and sufficient for stretch-induced reinforcement of stress fibers and growth of focal adhesions. Ca^{2+} activates several FA-associated proteins, including vinculin (91), Src family kinases (SFKs), talin (104) and MLC/Rho-Rho kinases (105). ~30% of $[Ca^{2+}]_{TM}$ signal induced by TRPV4 activation is subserved by secondary store release (23), suggesting that the mechanisms studied in the present work may include auxiliary contributions from Ca^{2+} stores and/or store-operated channels (106). Agents that induce Ca^{2+} release from intracellular stores similarly stimulate TM contractility and TGFβ1 signaling to augment the trabecular outflow resistance (35, 80, 107-108).

Our data demonstrate that mechanical stress has dramatic repercussions for the activation state, expression and localization of focal adaptor proteins. This process requires TRPV4 and calcium, as indicated by suppression of stretch-evoked increases in activated RhoA GTPase, paxillin (Tyr118), vinculin (Tyr1065) and zyxin (S142/143) phosphorylation (Figs. 3, 5, 7 & 9) by HC-06 and/or BAPTA-AM. The large early increases in paxillin phosphorylation, its sensitivity to local Ca^{2+} elevations and its localization to FAs point at paxillin as an initial target of increased strain. Consistent with this, TRPV4 inhibition and chelation of calcium suppressed stretch-dependent upregulation in paxillin phosphorylation, number of p-paxillin-ir sites and p-paxillin/pFAK-vinculin colocalization. The increased activation of paxillin and other FA proteins was generally not matched at the transcript level, suggesting that, within the time-frame of our experiments (1 – 7 hours), strain principally regulates FA remodeling through post-translational modifications. Paxillin activation was sensitive to TRPV4-mediated Ca^{2+} influx and ROCK, most likely via Rho-dependent "inside-out" changes in integrin affinity (109). Our finding that FAK migration to vinculin-containing sites and phosphorylation of zyxin acquire TRPV4-dependence after three hours of stretch, suggests that stress fiber enlargement, FA maturation and translocation of zyxin complexes into F-actin stress fibers involve additional Ca^{2+}-dependent steps that remain to be investigated. Potential effectors include the Ca^{2+}- calmodulin kinase II (CaMKII) which binds integrins upon increases in $[Ca^{2+}]_i$ (110, 111), prolongs the activation of RhoA (112) and regulates the tensile force in SMCs and myofibroblasts (113), stretch-sensitive Src family tyrosine kinases which bind TRPV4 and integrins, and the protein kinase C, which

regulates TGFβ1-dependent upregulation in F-actin and TM contractility (11, 80, 117). A potential caveat on the analysis side is that the substantial increase in the number of immunoreactive puncta in response to stretch might have resulted in the emergence of puncta that were too close for confocal resolution. Thus, we may have underestimated the magnitude of the effect.

A key question in glaucoma research concerns the molecular mechanisms through which elevations in IOP augment the TM resistance to aqueous outflow (65). Previous investigations tended to study the effects of stretch after >8 hours-to-days of stimulation (69, 118-121) however, we found that many key elements of force-induced TM remodeling and contractility are already in place at 1-3 hours of stretch. These include stress fiber upregulation, phosphorylation of RhoA, paxillin, FAK, vinculin and zyxin, and translocation of FA components (zyxin) (Figs. 2-9). Mature FAs contain myosin II directly participate in the contractile response to mechanical stress, which thus involves dynamic cooperation between ECM, membrane and cytoskeletal compartments.

Our findings are consistent with a model whereby TM cells rely on TRPV4 polymodality, Rho GTPases, integrins and Ca^{2+} to integrate parallel aspects of the mechanical and signaling milieu. These mechanisms may be homeostatic at short time scales as IOP fluctuates in response to ocular pulse, eye rubbing, saccades, blinking, swim goggles and yoga poses (65, 67) but become pathological in the presence of sustained stress when TM cells undergo myofibroblast transdifferentiation epitomized by TRPV4-dependent cytoskeletal stiffening, strengthened membrane-ECM contacts and increased contractility. Similar functions were ascribed to TRPV4 in SMC, endothelial, epithelial and mesenchymal remodeling during fibroproliferative cancer, lung and heart diseases (31, 33, 34, 122, 123), suggesting that the channel may participate in a universal program of tissue fibrosis and/or repair. TRPV4-Rho interactions identified here may also be relevant in the hypertensive posterior eye: TRPV4 is expressed in retinal ganglion cells, microglia, Müller cells and endothelial cells (32, 73, 126, 127) and glaucomatous optic nerve head shows elevated Rho GTPase levels (124). In addition to lowering IOP, ROCK inhibitor treatment also improved ganglion cell survival in glaucoma (125). In contrast to Y-2763, which triggers wholesale dissolution of F-actin (Fig. 2), TRPV4 antagonists have no observable side effects (23) and may be used to target the mechanotransducer to maintain function while preserving the cells' capacity for actomyosin regulation. Because the Rho pathway is

downstream of TRPV4, targeting the channel in the anterior and posterior eye could be a viable strategy that combines IOP-lowering with neuroprotection.

Acknowledgements

We thank Dr. Mary Beckerle (Huntsman Center, University of Utah) for actin and zyxin reagents and helpful discussions, and Dr. Amy Lin (Moran Eye Center, University of Utah) and Utah Lions Eye Bank for human tissue.

Conflict of Interest

The authors declare that they have no conflicts of interest with the contents of this article.

Author Contributions: Conception and design of research: M.L. and D.K.; conduction of the experiments: M.L.; data analysis: M.L.; interpretation of results: M.L. and D.K.; preparation of figures: M.L. and D.K; drafting of manuscript: M.L. and D.K., editing and revising the manuscript: M.L. and D.K.; approval of the final version of the manuscript: M.L. and D.K.

Funding was provided by the National Institutes of Health (R01EY027920, P30EY014800), Glaucoma Research Foundation, Willard L. Eccles Foundation, ALSAM-Skaggs Foundation, Neuroscience Initiative at the University of Utah and an Unrestricted Grant from Research to Prevent Blindness to the Department of Ophthalmology at the University of Utah.

Data Availability

All experimental data are contained within the manuscript.

References

1. Eyckmans J, Boudou T, Yu X, Chen CS. A hitchhiker's guide to mechanobiology. *Dev Cell.* 2011; 21: 35-47.
2. Katta S, Krieg M, Goodman MB. Feeling force: physical and physiological principles enabling sensory mechanotransduction. *Annu Rev Cell Dev Biol.* 2015; 31: 347-71.

3. Grosheva I, Vittitow JL, Goichberg P, Gabelt BT, Kaufman PL, Borrás T, Geiger B, Bershadsky AD. Caldesmon effects on the actin cytoskeleton and cell adhesion in cultured HTM cells. *Exp Eye Res.* 2006; 82: 945-58.
4. Tsai IJ, Chou CH, Yang YH, Lin WC, Lin YH, Chow LP, Lee HH, Kao PG, Liau WT, Jou TS, Tsau YK. Inhibition of Rho-associated kinase relieves C5a-induced proteinuria in murine nephrotic syndrome. *Cell Mol Life Sci.* 2015; 72: 3157-71.
5. Arora PD, Di Gregorio M, He P, McCulloch CA. TRPV4 mediates the Ca^{2+} influx required for the interaction between flightless-1 and non-muscle myosin, and collagen remodeling. *J Cell Sci.* 2017; 130: 2196-2208.
6. Livne A, Geiger B. The inner workings of stress fibers - from contractile machinery to focal adhesions and back. *J Cell Sci.* 2016; 129: 1293-304.
7. Kanchanawong P, Shtengel G, Pasapera AM, Ramko EB, Davidson MW, Hess HF, Waterman CM. Nanoscale architecture of integrin-based cell adhesions. *Nature.* 2010; 468: 580-4.
8. Arias-Salgado EG, Lizano S, Sarkar S, Brugge JS, Ginsberg MH, Shattil SJ. Src kinase activation by direct interaction with the integrin beta cytoplasmic domain. *Proc Natl Acad Sci U S A.* 2003; 100: 13298-302.
9. Sun Z, Guo SS, Fässler R. Integrin-mediated mechanotransduction. *J Cell Biol.* 2016; 215: 445-456.
10. Burridge K. Focal adhesions: a personal perspective on a half century of progress. *FEBS J.* 2017; 284: 3355-3361.
11. Wiederholt M, Thieme H, Stumpff F. The regulation of trabecular meshwork and ciliary muscle contractility. *Prog Retin Eye Res.* 2000; 19: 271-95.
12. Johnstone MA. The aqueous outflow system as a mechanical pump: evidence from examination of tissue and aqueous movement in human and non-human primates. *J Glaucoma.* 2004; 13: 421-38.
13. Gong H, Freddo TF. The washout phenomenon in aqueous outflow--why does it matter? *Exp Eye Res.* 2009; 88: 729-37.
14. Overby DR, Bertrand J, Schicht M, Paulsen F, Stamer WD, Lütjen-Drecoll E. The structure of the trabecular meshwork, its connections to the ciliary muscle, and the effect of pilocarpine on outflow facility in mice. *Invest Ophthalmol Vis Sci.* 2014; 55: 3727-36.

15. Welge-Lüssen U, May CA, Eichhorn M, Bloemendal H, Lütjen-Drecoll E. AlphaB-crystallin in the trabecular meshwork is inducible by transforming growth factor-beta. *Invest Ophthalmol Vis Sci.* 1999; 40: 2235-41.
16. Raghunathan VK, Benoit J, Kasetti R, Zode G, Salemi M, Phinney BS, Keller KE, Staverosky JA, Murphy CJ, Acott T, Vranka J. Glaucomatous cell derived matrices differentially modulate non-glaucomatous trabecular meshwork cellular behavior. *Acta Biomater.* 2018; 71: 444-459.
17. Li G, Lee C, Agrahari V, Wang K, Navarro I, Sherwood JM, Crews K, Farsiu S, Gonzalez P, Lin CW, Mitra AK, Ethier CR, Stamer WD. In vivo measurement of trabecular meshwork stiffness in a corticosteroid-induced ocular hypertensive mouse model. *Proc Natl Acad Sci U S A.* 2019; 116: 1714-1722.
18. Last JA, Pan T, Ding Y, Reilly CM, Keller K, Acott TS, Fautsch MP, Murphy CJ, Russell P. Elastic modulus determination of normal and glaucomatous human trabecular meshwork. *Invest Ophthalmol Vis Sci.* 2011; 52: 2147-52.
19. Pattabiraman PP, Inoue T, Rao PV. Elevated intraocular pressure induces Rho GTPase mediated contractile signaling in the trabecular meshwork. *Exp Eye Res.* 2015; 136: 29-33.
20. Vahabikashi A, Gelman A, Dong B, Gong L, Cha EDK., Schimmel M, Tamm ER, Perkumas K, Stamer WD, Sun C, Zhang HF, Gong H, Johnson M. Increased stiffness and flow resistance of the inner wall of Schlemm's canal in glaucomatous human eyes. *Proc Natl Acad Sci U S A.* 2019; pii: 201911837. doi: 10.1073/pnas.1911837116.
21. Peterson JA, Tian B, McLaren JW, Hubbard WC, Geiger B, Kaufman PL. Latrunculins' effects on intraocular pressure, aqueous humor flow, and corneal endothelium. *Invest Ophthalmol Vis Sci.* 2000; 41: 1749-58.
22. Rao PV, Pattabiraman PP, Kopczynski C. Role of the Rho GTPase/Rho kinase signaling pathway in pathogenesis and treatment of glaucoma: Bench to bedside research. *Exp Eye Res.* 2017; 158: 23-32.
23. Ryskamp DA, Frye AM, Phuong TT, Yarishkin O, Jo AO, Xu Y, Lakk M, Iuso A, Redmon SN, Ambati B, Hageman G, Prestwich GD, Torrejon KY, Križaj D. TRPV4 regulates calcium homeostasis, cytoskeletal remodeling, conventional outflow and intraocular pressure in the mammalian eye. *Sci Rep.* 2016; 6: 30583.

24. Yarishkin O, Phuong TTT, Križaj D. Trabecular Meshwork TREK-1 Channels Function as Polymodal Integrators of Pressure and pH. *Invest Ophthalmol Vis Sci.* 2019; 60: 2294-2303.
25. Yarishkin O, Baumann JM, Križaj D. Mechano-electrical transduction in trabecular meshwork involves parallel activation of TRPV4 and TREK-1 channels. *Channels (Austin).* 2019; 13: 168-171.
26. Luo N, Conwell MD, Chen X, Kettenhofen CI, Westlake CJ, Cantor LB, Wells CD, Weinreb RN, Corson TW, Spandau DF, Joos KM, Iomini C, Obukhov AG, Sun Y. Primary cilia signaling mediates intraocular pressure sensation. *Proc Natl Acad Sci U S A.* 2014; 111: 12871-6.
27. Ramadass R, Becker D, Jendrach M, Bereiter-Hahn J. Spectrally and spatially resolved fluorescence lifetime imaging in living cells: TRPV4-microfilament interactions. *Arch Biochem Biophys.* 2007; 463: 27-36.
28. Kida N, Sokabe T, Kashio M, Haruna K, Mizuno Y, Suga Y, Nishikawa K, Kanamaru A, Hongo M, Oba A, Tominaga M. Importance of transient receptor potential vanilloid 4 (TRPV4) in epidermal barrier function in human skin keratinocytes. *Pflugers Arch.* 2012; 463: 715-25.
29. Sokabe T, Fukumi-Tominaga T, Yonemura S, Mizuno A, Tominaga M. The TRPV4 channel contributes to intercellular junction formation in keratinocytes. *J Biol Chem.* 2010; 285: 18749-58.
30. Potla R, Hirano-Kobayashi M, Wu H, Chen H, Mammoto A, Matthews BD, Ingber DE. Molecular mapping of transmembrane mechanotransduction through the β1 integrin-CD98hc-TRPV4 axis. 2019; bioRxiv doi: https://doi.org/10.1101/617092
31. Rahaman SO, Grove LM, Paruchuri S, Southern BD, Abraham S, Niese KA, Scheraga RG, Ghosh S, Thodeti CK, Zhang DX, Moran MM, Schilling WP, Tschumperlin DJ, Olman MA. TRPV4 mediates myofibroblast differentiation and pulmonary fibrosis in mice. *J Clin Invest.* 2014; 124: 5225-38.
32. Phuong TTT, Redmon SN, Yarishkin O, Winter JM, Li DY, Križaj D. Calcium influx through TRPV4 channels modulates the adherens contacts between retinal microvascular endothelial cells. *J Physiol.* 2017; 595: 6869-6885.

33. Nam S, Gupta VK, Lee HP, Lee JY, Wisdom KM, Varma S, Flaum EM, Davis C, West RB, Chaudhuri O. Cell cycle progression in confining microenvironments is regulated by a growth-responsive TRPV4-PI3K/Akt-p27^{Kip1} signaling axis. *Sci Adv.* 2019; 5: eaaw6171.
34. Grove LM, Mohan ML, Abraham S, Scheraga RG, Southern BD, Crish JF, Naga Prasad SV, Olman MA. Translocation of TRPV4-PI3Kγ complexes to the plasma membrane drives myofibroblast transdifferentiation. *Sci Signal.* 2019; 12:607.
35. Rosenthal R, Choritz L, Schlott S, Bechrakis NE, Jaroszewski J, Wiederholt M, Thieme H. Effects of ML-7 and Y-27632 on carbachol- and endothelin-1-induced contraction of bovine trabecular meshwork. *Exp Eye Res.* 2005; 80: 837-45.
36. Krizaj D, Lakk M. Remodeling of focal adhesions and actin regulatory proteins in trabecular meshwork under tensile stress requires TRPV4-dependent Rho signaling *Invest. Ophthalmol. Vis. Sci.* 2019; 60: 5210.
37. Lakk M, Krizaj D. Mechanotransduction in trabecular meshwork cells requires obligatory interactions between TRPV4 channels, Rho signaling and focal adhesions. *Annual ASBMB Meeting,* San Diego. 2020. FASEB J 34(S1) 1-1.
38. Lapajne L, Lakk M, Yarishkin O, Gubeljak L, Hawlina M, Križaj D. Polymodal sensory transduction in mouse corneal epithelial cells. *Invest Ophthalmol Vis Sci.* 2020; 61: 1-14.
39. Hotulainen P, Lappalainen P. Stress fibers are generated by two distinct actin assembly mechanisms in motile cells. *J Cell Biol.* 2006; 173: 383-94.
40. Burridge K, Wennerberg K. Rho and Rac take center stage. *Cell.* 2004; 116: 167-79.
41. Guilluy C, Dubash AD, García-Mata R. Analysis of RhoA and Rho GEF activity in whole cells and the cell nucleus. *Nat Protoc.* 2011; 6: 2050-60.
42. Soine´ JR, Brand CA, Stricker J, Oakes PW, Gardel ML, Schwarz US. (2015) Model-based traction force microscopy reveals differential tension in cellular actin bundles. *PLoS Comput. Biol.* 2015; 11: e1004076.
43. Geiger B, Bershadsky A, Pankov R, Yamada KM. Transmembrane crosstalk between the extracellular matrix--cytoskeleton crosstalk. *Nat Rev Mol Cell Biol.* 2001; 2: 793-805.
44. Calalb MB, Polte TR, Hanks SK. Tyrosine phosphorylation of focal adhesion kinase at sites in the catalytic domain regulates kinase activity: a role for Src family kinases. *Mol Cell Biol.* 1995; 15: 954-63.

45. Seong J, Tajik A, Sun J, Guan JL, Humphries MJ, Craig SE, Shekaran A, García AJ, Lu S, Lin MZ, Wang N, Wang Y. Distinct biophysical mechanisms of focal adhesion kinase mechanoactivation by different extracellular matrix proteins. *Proc Natl Acad Sci U S A.* 2013; 110: 19372-7.
46. Schlunck G, Han H, Wecker T, Kampik D, Meyer-ter-Vehn T, Grehn F. Substrate rigidity modulates cell matrix interactions and protein expression in human trabecular meshwork cells. *Invest Ophthalmol Vis Sci.* 2008; 49: 262-9.
47. Gagen D, Filla MS, Clark R, Liton P, Peters DM. Activated αvβ3 integrin regulates αvβ5 integrin-mediated phagocytosis in trabecular meshwork cells. *Invest Ophthalmol Vis Sci.* 2013; 54: 5000-11.
48. Kwon HS, Tomarev SI. Myocilin, a glaucoma-associated protein, promotes cell migration through activation of integrin-focal adhesion kinase-serine/threonine kinase signaling pathway. *J Cell Physiol.* 2011; 226: 3392-402.
49. O'Brien ET, Kinch M, Harding TW, Epstein DL. A mechanism for trabecular meshwork cell retraction: ethacrynic acid initiates the dephosphorylation of focal adhesion proteins. *Exp Eye Res.* 1997; 65: 471-83.
50. Schaller MD, Hildebrand JD, Shannon JD, Fox JW, Vines RR, Parsons JT. Autophosphorylation of the focal adhesion kinase, pp125FAK, directs SH2-dependent binding of pp60src. *Mol Cell Biol.* 1994; 14: 1680-8.
51. Zhou L, Cheng EL, Rege P, Yue BY. Signal transduction mediated by adhesion of human trabecular meshwork cells to extracellular matrix. *Exp Eye Res.* 2000; 70: 457-65.
52. Zaidel-Bar R, Geiger B. The switchable integrin adhesome. *J Cell Sci.* 2010; 123: 1385-8.
53. Giannone G. Super-resolution links vinculin localization to function in focal adhesions. *Nat Cell Biol.* 2015; 17: 845-7.
54. Sinnett-Smith J, Lunn JA, Leopoldt D, Rozengurt E. Y-27632, an inhibitor of Rho-associated kinases, prevents tyrosine phosphorylation of focal adhesion kinase and paxillin induced by bombesin: dissociation from tyrosine phosphorylation of p130(CAS). *Exp Cell Res.* 2001; 266: 292-302.
55. Auernheimer V, Lautscham LA, Leidenberger M, Friedrich O, Kappes B, Fabry B, Goldmann WH. Vinculin phosphorylation at residues Y100 and Y1065 is required for cellular force transmission. *J Cell Sci.* 2015; 128: 3435-43.

56. Yi J, Kloeker S, Jensen CC, Bockholt S, Honda H, Hirai H, Beckerle MC. Members of the Zyxin family of LIM proteins interact with members of the p130Cas family of signal transducers. *J Biol Chem.* 2002; 277: 9580-9.
57. Hoffman LM, Jensen CC, Chaturvedi A, Yoshigi M, Beckerle MC. (2012) Stretch-induced actin remodeling requires targeting of zyxin to stress fibers and recruitment of actin regulators. *Mol Biol Cell.* 2012; 23: 1846-59.
58. Bollinger KE, Crabb JS, Yuan X, Putliwala T, Clark AF, Crabb JW. Quantitative proteomics: TGFβ_2 signaling in trabecular meshwork cells. *Invest Ophthalmol Vis Sci.* 2011; 52: 8287-94.
59. Montecchi-Palmer M, Bermudez JY, Webber HC, Patel GC, Clark AF, Mao W. TGFβ2 Induces the Formation of Cross-Linked Actin Networks (CLANs) in Human Trabecular Meshwork Cells Through the Smad and Non-Smad Dependent Pathways. *Invest Ophthalmol Vis Sci.* 2017; 58: 1288-1295.
60. Yoshigi M, Hoffman LM, Jensen CC, Yost HJ, Beckerle MC. Mechanical force mobilizes zyxin from focal adhesions to actin filaments and regulates cytoskeletal reinforcement. *J Cell Biol.* 2005; 171: 209-15.
61. Ngu H, Feng Y, Lu L, Oswald SJ, Longmore GD, Yin FC. Effect of focal adhesion proteins on endothelial cell adhesion, motility and orientation response to cyclic strain. *Ann Biomed Eng.* 2010; 8: 208-22.
62. Fabry B, Klemm AH, Kienle S, Schäffer TE, Goldmann WH. Focal adhesion kinase stabilizes the cytoskeleton. *Biophys J.* 2011; 101: 2131-8.
63. Grierson I, Lee WR. The fine structure of the trabecular meshwork at graded levels of intraocular pressure. (2) Pressures outside the physiological range (0 and 50 mmHg). *Exp Eye Res.* 1975; 20: 523-30.
64. Downs JC, Burgoyne CF, Seigfreid WP, Reynaud JF, Strouthidis NG, Sallee V. 24-hour IOP telemetry in the nonhuman primate: implant system performance and initial characterization of IOP at multiple timescales. *Invest Ophthalmol Vis Sci.* 2011; 52: 7365-75.
65. Sherwood JM, Stamer WD, Overby DR. A model of the oscillatory mechanical forces in the conventional outflow pathway. *J R Soc Interface.* 2019; 16: 20180652.
66. Ramos RF, Sumida GM, Stamer WD. Cyclic mechanical stress and trabecular meshwork cell contractility. *Invest Ophthalmol Vis Sci.* 2009; 50: 3826-32.

67. Turner DC, Edmiston AM, Zohner YE, Byrne KJ, Seigfreid WP, Girkin CA, Morris JS, Downs JC. Transient Intraocular Pressure Fluctuations: Source, Magnitude, Frequency, and Associated Mechanical Energy. *Invest Ophthalmol Vis Sci.* 2019; 60: 2572-2582.
68. Tamm ER, Siegner A, Baur A, Lütjen-Drecoll E. Transforming growth factor-beta 1 induces alpha-smooth muscle-actin expression in cultured human and monkey trabecular meshwork. *Exp Eye Res.* 1996; 62: 389-97.
69. Tumminia SJ, Mitton KP, Arora J, Zelenka P, Epstein DL, Russell P. Mechanical stretch alters the actin cytoskeletal network and signal transduction in human trabecular meshwork cells. *Invest Ophthalmol Vis Sci.* 1998; 39: 1361-71.
70. Ramos RF, Stamer WD. Effects of cyclic intraocular pressure on conventional outflow facility. *Invest Ophthalmol Vis Sci.* 2008; 49; 275-81.
71. WuDunn D. Mechanobiology of trabecular meshwork cells. *Exp Eye Res.* 2009; 88: 718-23.
72. Pattabiraman PP, Rao PV. Mechanistic basis of Rho GTPase-induced extracellular matrix synthesis in trabecular meshwork cells. *Am J Physiol Cell Physiol.* 2010; 298: C749-63.
73. Križaj D. What is glaucoma? *Webvision: The Organization of the Retina and Visual System [Internet]*. 2019. University of Utah Health Sciences Center, Salt Lake City, UT
74. Honjo M, Tanihara H, Inatani M, Kido N, Sawamura T, Yue BY, Narumiya S, Honda Y. Effects of rho-associated protein kinase inhibitor Y-27632 on intraocular pressure and outflow facility. *Invest Ophthalmol Vis Sci.* 2001; 42: 137-44.
75. Epstein DL, Rowlette LL, Roberts BC. Acto-myosin drug effects and aqueous outflow function. *Invest Ophthalmol Vis Sci.* 1999; 40: 74-81.
76. Ethier CR, Read AT, Chan DW. Effects of latrunculin-B on outflow facility and trabecular meshwork structure in human eyes. *Invest Ophthalmol Vis Sci.* 2006; 47: 1991-8.
77. Vittitow JL, Garg R, Rowlette LL, Epstein DL, O'Brien ET, Borrás T. Gene transfer of dominant-negative RhoA increases outflow facility in perfused human anterior segment cultures. *Mol Vis.* 2002; 8: 32-44.
78. Pattabiraman PP, Maddala R, Rao PV. Regulation of plasticity and fibrogenic activity of trabecular meshwork cells by Rho GTPase signaling. *J Cell Physiol*. 2014; 229: 927-42.
79. Wakabayashi S, Morihara H, Yokoe S, Nakagawa T, Moriwaki K, Tomoda K, Asahi M. Overexpression of Na^+/H^+ exchanger 1 specifically induces cell death in human iPS cells via sustained activation of the Rho kinase ROCK. *J Biol Chem.* 2019; 294: 19577-19588.

80. Nakamura Y, Hirano S, Suzuki K, Seki K, Sagara T, Nishida T. Signaling mechanism of TGF-beta1-induced collagen contraction mediated by bovine trabecular meshwork cells. *Invest Ophthalmol Vis Sci.* 2002; 43: 3465-72.
81. Junglas B, Kuesper S, Seleem AA, Struller T, Ullmann S, Bösl M, Bosserhoff A, Köstler J, Wagner R, Tamm ER, Fuchshofer R. Connective tissue growth factor causes glaucoma by modifying the actin cytoskeleton of the trabecular meshwork. *Am J Pathol.* 2012; 180: 2386-403.
82. LeBleu VS, Taduri G, O'Connell J, Teng Y, Cooke VG, Woda C, Sugimoto H, Kalluri R. Origin and function of myofibroblasts in kidney fibrosis. *Nat Med.* 2013; 19: 1047-53.
83. Loukin S, Zhou X, Su Z, Saimi Y, Kung C. Wild-type and brachyolmia-causing mutant TRPV4 channels respond directly to stretch force. *J Biol Chem.* 2010; 285: 27176-81.
84. Servin-Vences MR, Moroni M, Lewin GR, Poole K. Direct measurement of TRPV4 and PIEZO1 activity reveals multiple mechanotransduction pathways in chondrocytes. *Elife.* 2017; 6: pii: e21074.
85. Strotmann R, Harteneck C, Nunnenmacher K, Schultz G, Plant TD. OTRPC4, a nonselective cation channel that confers sensitivity to extracellular osmolarity. *Nat Cell Biol.* 2000; 2: 695-702.
86. Jo AO, Lakk M, Frye AM, Phuong TT, Redmon SN, Roberts R, Berkowitz BA, Yarishkin O, Križaj D. Differential volume regulation and calcium signaling in two ciliary body cell types is subserved by TRPV4 channels. *Proc Natl Acad Sci U S A.* 2016; 113: 3885-90.
87. Toft-Bertelsen TL, Križaj D, MacAulay N. When size matters: transient receptor potential vanilloid 4 channel as a volume-sensor rather than an osmo-sensor. *J Physiol.* 2017; 595: 3287-3302.
88. Köhler R, Hoyer J. Role of TRPV4 in the Mechanotransduction of Shear Stress in Endothelial Cells. In: *TRP Ion Channel Function in Sensory Transduction and Cellular Signaling Cascades. Boca Raton (FL): CRC Press/Taylor & Francis;* Frontiers in Neuroscience. 2007. Chapter 27.
89. Baratchi S, Knoerzer M, Khoshmanesh K, Mitchell A, McIntyre P. Shear Stress Regulates TRPV4 Channel Clustering and Translocation from Adherens Junctions to the Basal Membrane. *Sci Rep.* 2017; 7: 15942.

90. Matthews BD, Thodeti CK, Tytell JD, Mammoto A, Overby DR, Ingber DE. Ultra-rapid activation of TRPV4 ion channels by mechanical forces applied to cell surface beta1 integrins. *Integr Biol (Camb).* 2010; 2: 435-42.
91. Gilchrist CL, Leddy HA, Kaye L, Case ND, Rothenberg KE, Little D, Liedtke W, Hoffman BD, Guilak F. TRPV4-mediated calcium signaling in mesenchymal stem cells regulates aligned collagen matrix formation and vinculin tension. *Proc Natl Acad Sci U S A.* 2019; 116: 1992-1997.
92. Coste B, Mathur J, Schmidt M, Earley TJ, Ranade S, Petrus MJ, Dubin AE, Patapoutian A. Piezo1 and Piezo2 are essential components of distinct mechanically activated cation channels. *Science.* 2010; 330: 55-60.
93. Brohawn SG, Campbell EB, MacKinnon R. Physical mechanism for gating and mechanosensitivity of the human TRAAK K+ channel. *Nature.* 2014; 516: 126-30.
94. Vriens J, Watanabe H, Janssens A, Droogmans G, Voets T, Nilius B. Cell swelling, heat, and chemical agonists use distinct pathways for the activation of the cation channel TRPV4. *Proc Natl Acad Sci U S A.* 2004; 101: 396-401.
95. White JP, Cibelli M, Urban L, Nilius B, McGeown JG, Nagy I. TRPV4: Molecular Conductor of a Diverse Orchestra. *Physiol Rev.* 2016; 96: 911-73.
96. Toft-Bertelsen TL, Yarishkin O, Redmon S, Phuong TTT, Križaj D, MacAulay N. Volume sensing in the transient receptor potential vanilloid 4 ion channel is cell type-specific and mediated by an N-terminal volume-sensing domain. *J Biol Chem.* 2019; 294: 18421-18434.
97. Berna-Erro A, Izquierdo-Serra M, Sepúlveda RV, Rubio-Moscardo F, Doñate-Macián P, Serra SA, Carrillo-Garcia J, Perálvarez-Marín A, González-Nilo F, Fernández-Fernández JM, Valverde MA. Structural determinants of 5',6'-epoxyeicosatrienoic acid binding to and activation of TRPV4 channel. *Sci Rep.* 2017; 7: 10522.
98. Ryskamp DA, Jo AO, Frye AM, Vazquez-Chona F, MacAulay N, Thoreson WB, Križaj D. Swelling and eicosanoid metabolites differentially gate TRPV4 channels in retinal neurons and glia. *J Neurosci.* 2014; 34: 15689-700.
99. Luna C, Li G, Qiu J, Challa P, Epstein DL, Gonzalez P. Extracellular release of ATP mediated by cyclic mechanical stress leads to mobilization of AA in trabecular meshwork cells. *Invest Ophthalmol Vis Sci.* 2009; 50: 5805-10.

100. Zhou L, Maruyama I, Li Y, Cheng EL, Yue BY. Expression of integrin receptors in the human trabecular meshwork. *Curr Eye Res.* 1999; 19: 395-402.

101. Xiong S, Xu Y, Wang Y, Kumar A, Peters DM, Du Y. α5β1 Integrin Promotes Anchoring and Integration of Transplanted Stem Cells to the Trabecular Meshwork in the Eye for Regeneration. *Stem Cells Dev.* 2020; 29: 290-300.

102. Filla MS, Faralli JA, Peotter JL, Peters DM. The role of integrins in glaucoma. *Exp Eye Res.* 2017; 158: 124-136.

103. Faralli JA, Filla MS, Peters DM. Effect of αvβ3 Integrin Expression and Activity on Intraocular Pressure. *Invest Ophthalmol Vis Sci.* 2019; 60: 1776-1788.

104. Kerstein PC, Jacques-Fricke BT, Rengifo J, Mogen BJ, Williams JC, Gottlieb PA, Sachs F, Gomez TM. Mechanosensitive TRPC1 channels promote calpain proteolysis of talin to regulate spinal axon outgrowth *J Neurosci*. 2013; 33: 273-85.

105. Sakurada S, Takuwa N, Sugimoto N, Wang Y, Seto M, Sasaki Y, Takuwa Y. Ca2+-dependent activation of Rho and Rho kinase in membrane depolarization-induced and receptor stimulation-induced vascular smooth muscle contraction. *Circ Res.* 2003; 93: 548-56.

106. Abad E, Lorente G, Gavara N, Morales M, Gual A, Gasull X. Activation of store-operated Ca(2+) channels in trabecular meshwork cells. *Invest Ophthalmol Vis Sci.* 2008; 49: 677-86.

107. Sumida GM, Stamer WD. $S1P_2$ receptor regulation of sphingosine-1-phosphate effects on conventional outflow physiology. *Am J Physiol Cell Physiol.* 2011; 300: C1164-71.

108. Boussommier-Calleja A, Bertrand J, Woodward DF, Ethier CR, Stamer WD, Overby DR. Pharmacologic manipulation of conventional outflow facility in ex vivo mouse eyes. *Invest Ophthalmol Vis Sci.* 2012; 53: 5838-45. .

109. Laudanna C, Campbell JJ, Butcher EC. Role of Rho in chemoattractant-activated leukocyte adhesion through integrins. *Science.* 1996; 271: 981-3.

110. Strotmann R, Schultz G, Plant TD. Ca2+-dependent potentiation of the nonselective cation channel TRPV4 is mediated by a C-terminal calmodulin binding site. *J Biol Chem.* 2003; 278: 26541-9.

111. Goswami C, Kuhn J, Heppenstall PA, Hucho T. Importance of non-selective cation channel TRPV4 interaction with cytoskeleton and their reciprocal regulations in cultured cells. *PLoS One.* 2010; 5: e11654.

112. Murakoshi H, Wang H, Yasuda R. Local, persistent activation of Rho GTPases during plasticity of single dendritic spines. *Nature.* 2011; 472: 100-4.

113. Tojkander S, Ciuba K, Lappalainen P. CaMKK2 Regulates Mechanosensitive Assembly of Contractile Actin Stress Fibers. *Cell Rep.* 2018; 24: 11-19.

114. Wang H, Chumnarnsilpa S, Loonchanta A, Li Q, Kuan YM, Robine S, Larsson M, Mihalek I, Burtnick LD, Robinson RC. Helix straightening as an activation mechanism in the gelsolin superfamily of actin regulatory proteins. *J Biol Chem.* 2009; 284: 21265-9.

115. Bourguignon LY, Gilad E, Brightman A, Diedrich F, Singleton P. Hyaluronan-CD44 interaction with leukemia-associated RhoGEF and epidermal growth factor receptor promotes Rho/Ras co-activation, phospholipase C epsilon-Ca2+ signaling, and cytoskeleton modification in head and neck squamous cell carcinoma cells. *J Biol Chem.* 2006; 281: 14026-40.

116. Rattan S. Ca2+/calmodulin/MLCK pathway initiates, and RhoA/ROCK maintains, the internal anal sphincter smooth muscle tone. *Am J Physiol Gastrointest Liver Physiol.* 2017; 312: G63-G66.

117. Kirihara T, Shimazaki A, Nakamura M, Miyawaki N. Ocular hypotensive efficacy of Src-family tyrosine kinase inhibitors via different cellular actions from Rock inhibitors. *Exp Eye Res.* 2014; 119: 97-105.

118. Borrás T. Gene expression in the trabecular meshwork and the influence of intraocular pressure. *Prog Retin Eye Res.* 2003; 22: 435-63.

119. Vittal V, Rose A, Gregory KE, Kelley MJ, Acott TS. Changes in gene expression by trabecular meshwork cells in response to mechanical stretching. *Invest Ophthalmol Vis Sci.* 2005; 46: 2857-68.

120. Baetz NW, Hoffman EA, Yool AJ, Stamer WD. Role of aquaporin-1 in trabecular meshwork cell homeostasis during mechanical strain. *Exp Eye Res.* 2009; 89: 95-100.

121. Bradley JM, Kelley MJ, Rose A, Acott TS. Signaling pathways used in trabecular matrix metalloproteinase response to mechanical stretch. *Invest Ophthalmol Vis Sci.* 2003; 44: 5174-81.

122. Adapala RK, Thoppil RJ, Luther DJ, Paruchuri S, Meszaros JG, Chilian WM, Thodeti CK. TRPV4 channels mediate cardiac fibroblast differentiation by integrating mechanical and soluble signals. *J Mol Cell Cardiol.* 2013; 54: 45-52.

123. Sharma S, Goswami R, Zhang DX, Rahaman SO. TRPV4 regulates matrix stiffness and TGFβ1-induced epithelial-mesenchymal transition. *J Cell Mol Med.* 2019; 23: 761-774.

124. Goldhagen B, Proia AD, Epstein DL, Rao PV. Elevated levels of RhoA in the optic nerve head of human eyes with glaucoma. *J Glaucoma.* 2012; 21: 530-8.

125. Yamamoto K, Maruyama K, Himori N, Omodaka K, Yokoyama Y, Shiga Y, Morin R, Nakazawa T. The novel Rho kinase (ROCK) inhibitor K-115: a new candidate drug for neuroprotective treatment in glaucoma. *Invest Ophthalmol Vis Sci.* 2014; 55: 7126-36.

126. Ryskamp DA, Witkovsky P, Barabas P, Huang W, Koehler C, Akimov NP, Lee SH, Chauhan S, Xing W, Rentería RC, Liedtke W, Krizaj D. The polymodal ion channel transient receptor potential vanilloid 4 modulates calcium flux, spiking rate, and apoptosis of mouse retinal ganglion cells. *J Neurosci.* 2011; 31: 7089-101.

127. Jo AO, Ryskamp DA, Phuong TT, Verkman AS, Yarishkin O, MacAulay N, Križaj D. TRPV4 and AQP4 Channels Synergistically Regulate Cell Volume and Calcium Homeostasis in Retinal Müller Glia. *J Neurosci.* 2015; 35: 13525-37.

128. Lakk M, Young D, Baumann JM, Jo AO, Hu H, Križaj D. Polymodal TRPV1 and TRPV4 Sensors Colocalize but Do Not Functionally Interact in a Subpopulation of Mouse Retinal Ganglion Cells. *Front Cell Neurosci.* 2018; 12: 353.

129. Lakk M, Yarishkin O, Baumann JM, Iuso A, Križaj D. Cholesterol regulates polymodal sensory transduction in Müller glia. *Glia.* 2017; 65: 2038-2050.

Tables

Table 1. Primer sequences used for PCR analysis

Name	*Forward primer*	*Reverse primer*	*NCBI reference number*
Myocilin	CCACGTGGAGAATCGACACA	TCCAGTGGCCTAGGCAGTAT	NM_000261.1
Timp3	CAAGATGTACACGGGGCTGT	AGGCGTAGTGTTTGGACTGG	NM_000362.4
AQP1	TGGAGCAAGCTCTTCCCTTG	CTGTCCTTGGGCTGCAACTA	NM_198098.3
MGP	CTCTCTCTGAACTGGCATCGT	TATTGAGCTCGTGGACAGGC	NM_001190839.1
Acta2	GTCACCCACAATGTCCCCAT	GGAATAGCCACGCTCAGTCA	NM_001141945.2
Zyxin	ACTACCACAAGCAGTACGCC	GAAGTTCTTGTCCAGGGCGA	NM_003461.4
FAK	ATGGCTGGCAGCATCTATC	TTCCTGTTGCTGTCGGATTAG	NM_153831.3
RhoA	GCGCTTTTGGGTACATGGAG	TTCCCACGTCTAGCTTGCAG	NM_001664.3
Vinculin	AGGAGCACCGAGTGATGTTG	TCAGTGTCCTTCTTGCTGGC	M33308.1
Paxillin	AGTGTGGAGCCTTCTTTGG	CGTGTTGAGGGCTGAGATATAG	NM_002859.3
GAPDH	CTCCTGTTCGACAGTCAGCC	GACTCCGACCTTCACCTTCC	NM_002046.5
β-tubulin	CCTTCCTCCACTGGTACAC	TCTGCCTTAGGCCTCCTCTT	AF141349.1

Table 2. Primary antibodies *(WB, Western blots; ICC, immunocytochemistry)*

Name	*Specificity*	*Host*	*Dilution*	*Source*
Zyxin	Total zyxin protein	rabbit	1:2000 (WB) 1:1000 (ICC)	Sigma-Aldrich Z4751
Phospho-zyxin	Zyxin, phosphorylated at Ser142, Ser143 or both	rabbit	1:1000 (WB)	Cell Signaling #4863
FAK	Total FAK	rabbit	1:1000 (WB) 1:500 (ICC)	Abcam EP695Y
Phospho-FAK	FAK, phosphorylated at Y397	rabbit	1:1000 (WB) 1:500 (ICC)	Abcam EP2160Y
Vinculin	Total vinculin	rabbit mouse	1:1000 (WB) 1:4000 (ICC)	Cell Signaling #4650 Sigma-Aldrich V9131
Phospho-vinculin	Vinculin, phosphorylated at Tyr1065	rabbit	1:500 (WB) 1:250 (ICC)	Thermo Fisher 44-1078
Paxillin	Total Paxillin	rabbit	1:1000 (WB)	Cell Signaling #12065
Phospho-paxillin	Paxillin, phosphorylated at Tyr118	rabbit	1:1000 (WB)	Cell Signaling #2541
Phospho-paxillin	Paxillin, phosphorylated at Tyr31	rabbit	1:250 (ICC)	Abcam ab4832
Myocilin	Total myocilin (276-290)	rabbit	1:500 (WB) 1:250 (ICC)	Sigma-Aldrich SAB1101183
GAPDH (HRP)	Glyceraldehyde 3-phosphate dehydrogenase	rabbit	1:5000 (WB)	Abcam EPR6256
Phalloidin-Alexa 488	F-actin marker		1:1000 (ICC)	Thermo Fisher A12379

Figure Legends

Figure 1. Stretch-induced upregulation of actin cytoskeleton in human trabecular meshwork (hTM) cells requires TRPV4 and ROCK activation. (A) F-actin labeled with phalloidin- Alexa 488 nm and (B) averaged data (N = 4). Preparations were stimulated for 1 hour with 6% cyclic stretch in the presence/absence of TRPV4/ROCK inhibitors. Stretch-induced increases in stress fiber fluorescence were suppressed by HC-06 (1 µM) and Y-27632 (10 µM). Exposure to the antagonists alone had no significant effect on stress fiber formation. Low magnification images are shown in Supplementary Fig. 1A.Scale bar: 20 µm. *, $P < 0.05$, **, $P < 0.01$.

Figure 2. ROCK signaling is downstream from TRPV4. (A - C) Cytosolic Ca^{2+} signals (*left panel*s) and live actin fluorescence (*right panels*) were measured concurrently in Fura-2 AM-loaded cells. (A) GSK101 induced $[Ca^{2+}]_i$ elevations and reversibly stimulated stress fiber formation (panel ii) in the representative cell (n = 4). (Bi-iii) Y-27632 had no significant effect on baseline $[Ca^{2+}]_i$ and resting stress fiber formation (n = 4) (Supplementary Fig. 2A). (C) Y-27632 does not affect the amplitude of GSK101-evoked $[Ca^{2+}]_i$ elevations, however (Ci-iii) Y-27632 significantly (Supplementary Fig. 2A) reduces stress fiber fluorescence (n = 4). (D) Averaged $[Ca^{2+}]_i$ data from Fura-2 AM-loaded cells (n = 52-162, N = 4). (E) Representative traces and averaged results for 30 min stretched (black trace, bars) and Y-27632-treated (10 µM, red trace, bars) TM cells. $[Ca^{2+}]_i$ responses induced by stretch are independent of Y-27632. ****, $P < 0.0001$; N.S., non-significant.

Figure 3. Stretch-induced stimulation of TRPV4 activates RhoA. (A) Semiquantitative RT-PCR, shown as ~fold *RhoA* mRNA following 1 – 7 hours of stretch. *RhoA* mRNA levels transiently increased after 1 hour biaxial stretch (3.00 ± 0.72; N = 4). (B & C) Western blot; active (GTP-bound) Rho protein levels were increased at 1 hour stretch (1.56 ± 0.12; N = 3) whereas the inactive (GDP-bound) Rho levels were unaffected. HC-06 but not Y-27632, suppressed RhoA protein upregulation. *, $P < 0.05$.

Figure 4. TRPV4 and Rho-signaling time-dependently modulate stretch-induced phosphorylation of Focal Adhesion Kinase (FAK). (A) RT-PCR as ~fold *FAK* mRNA. Strain

increases *FAK* mRNA levels at 3 hrs (1.57 ± 0.12-fold; N = 3). (B - D) Western blot data. (B) Total FAK protein levels remain constant, while FAK Tyr397 phosphorylation increases following 1 and 3 hour strain exposure (2.11 ± 0.07 and 2.28 ± 0.16, respectively; N = 3-5). (C & D) pFAK upregulation at 1 hour is inhibited by Y-27632 (0.88 ± 0.14; N = 3) but not HC-06, whereas 3 hour stretch effect is blocked by both antagonists (N = 3-5). *, $P < 0.05$, **, $P < 0.01$.

Figure 5. Stretch-induced paxillin phosphorylation requires TRPV4. (A) Semiquantitative RT-PCR, with ~fold changes of *paxillin* mRNA for 1 - 7 hour stretch (N = 3). (B - D) Western blots. (B) Stretch triggers an early elevation of activated (Tyr118) vs. nonactivated forms of the protein (N =3). (C) Western blot for total paxillin in control and stretched samples at 1-7 hours. (Di-ii) Western blot and averaged data for activated paxillin at 1 hour stretch, in the presence of HC-06, Y-27632 or BAPTA. The stretch effect is blocked by HC-06 and the calcium chelator BAPTA (N = 3). (E) Control (i) and stretched (ii) TM cells immunolabeled for p-paxillin, in the presence/absence of BAPTA (iii), HC-06 (iv), or Y-27632 (v). Stretch promotes the dispersal of p-paxillin towards distal membrane sites; TRPV4 and Rho inhibition lowers the extent and dispersion of active paxillin signals. (F) The number of p-paxillin (Tyr31) particuli is upregulated after 1 hour stretch in a TRPV4-, BAPTA- and ROCK-dependent manner, whereas the levels of total vinculin remain unchanged. (G) Colocalization between vinculin and p-paxillin increases in TRPV4- and Rho-dependent manner. *, $P < 0.05$, **, $P < 0.01$.

Figure 6. Biaxial stretch facilitates vinculin - pFAK colocalization. (A) Semiquantitative RT-PCR, ~fold changes of *vinculin* mRNA for 1 – 7 hour stretch durations. (B) Western blots. Stretch has no effect on total vinculin protein levels. (C) Control and stretched TM cells in the presence/absence of HC-06 or Y-27632, immunolabeled for total vinculin and pFAK. Averaged data are shown in (D-G). (D & F) 1 hour of stretch upregulates the number of pFAK particuli in a ROCK-dependent manner, and increases the extent of colocalization with vinculin. (E & G) 3 hours of stretch increase pFAK levels and its colocalization with vinculin; this effect is blocked by both HC-06 and Y-27632. *, $P < 0.05$; **, $P < 0.01$; ***, $P < 0.001$. Scale bar: 20 µm.

Figure 7. Stretch-induced vinculin phosphorylation requires TRPV4 and Rho signaling. Exposure to strain increases the p-vinculin particulum numbers together with the particulum size

of total protein. These effects are suppressed by TRPV4 and ROCK inhibitors. (A) Inverted images of total vinculin immunoreactivity in control, stretch- and antagonist-treated cells. (B) Averaged particulum size of total vinculin in stretched cells in the presence/absence of blockers plotted relative to averaged value in unstimulated cells. The S.E.M. denote variance across separate experiments. (C) Inverted images of Tyr1065-phosphorylated vinculin immunoreactivity in control, stretch- and antagonist-treated cells. (D) Averaged particulum size of activated vinculin in stretched cells in the presence/absence of blockers plotted relative to averaged value in unstimulated cells. N = 3; n = 50-100 cells; *, $P < 0.05$; **, $P < 0.01$.

Figure 8. TRPV4 and Rho-signaling time-dependently modulate stretch-induced phosphorylation of zyxin. (A) Semiquantitative RT-PCR. *Zyxin* mRNA is significantly increased at 1 - 5 hours stretch (N = 3-4). (B - E) Western blots. (B) Cyclic stretch triggers increases phosphorylated zyxin protein at 1 and 3 hours (N = 3-4). (Ci) Total zyxin protein in control and stretch samples at 1 – 7 hours. (Cii) Activated zyxin protein in the presence/absence of stretch and TRPV4/ROCK inhibition. Stretch augments zyxin/p-zyxin expression (D) Averaged data for experiments shown in Cii (N = 3-5). Stretch-induced upregulation in p-zyxin is suppressed by HC-06 and Y-27632 at 3 but not 1, hours. (Ei-ii) BAPTA-AM does not affect p-zyxin levels in the presence of stretch (N = 3). *, $P < 0.05$; **, $P < 0.01$; N.S. = non-significant.

Figure 9. Mechanical force-induced translocation of zyxin requires TRPV4 and Rho signaling. Double labeling for F-actin and total zyxin. 1- hour stretch increases zyxin-ir and promotes its translocation into stress fibers. Stretch-induced translocation of zyxin is inhibited by HC-06 and Y-27632. In the presence of Y-27632, zyxin appears to favors membrane locations (N = 3). Scale bar: 20 µm.

Supplementary Figure 1. TRPV4 activation and Rho signaling have no effect on TM cell shape or viability. (A) Representative, low magnification images of cells labeled with phalloidin actin-Alexa 488 nm and DAPI. Y-27632 and HC-06 has no effect on cell and nuclear shape. Stretch upregulates F-actin in a ROCK- and TRPV4-dependent manner without impacting the overall shape (B) Double labeling for F-actin and the fluorogenic SRB-VAD-FMK caspase probe shows rare positive signals seen as cells that lost cytoplasm (white arrow). (C) SRB-VAD-

FMK+ signals across cohorts (n = 363-431; N = 2) were normalized to controls. The experimental conditions did not show significant differences from controls. Scale bar: 50 µm.

Supplementary Figure 2. ROCK signaling is downstream from TRPV4. (A) Averaged data for experiments shown in Figure 2Ai-iii-Ci-iii. Y-27632 alone had no significant effect resting stress fiber fluorescence, however Y-27632 significantly prevent GSK 101 effect on stress fiber formation (B) Averaged data for 15 min stretched (black bars) and Y-27632-treated (10 µM, red bars) TM cells (n = 30; N = 4). Stretch-evoked $[Ca^{2+}]_i$ responses are independent of Y-27632. *, $P < 0.05$; ****, $P < 0.0001$; N.S., non-significant.

Supplementary Figure 3. Stretch-induced paxillin phosphorylation requires TRPV4. Control and stretched TM cells in the presence/absence of BAPTA, HC-06 or Y-27632, immunolabeled for p-paxillin (Tyr31) and total vinculin. The number of p-paxillin (Tyr31) particuli is upregulated after 1 hour stretch in a TRPV4-, BAPTA- and ROCK-dependent manner, whereas the levels of total vinculin remain unchanged. Colocalization between vinculin and p-paxillin increases in TRPV4- and Rho-dependent manner. Averaged data shown in Figure 5F and G. N = 3; Scale bar: 20 µm.

Supplementary Figure 4. Stretch-induced vinculin phosphorylation requires TRPV4 and Rho signaling. (A) Immunolabeling for total vinculin protein and (B) for Tyr1065-phosphorylated vinculin. Exposure to strain increases the p-vinculin particulum numbers at 1 hour together with the particulum size of total protein. These effects are suppressed by TRPV4 and ROCK inhibitors. Averaged, normalized data shown in Figure 7B and D. N = 3; *, $P < 0.05$; **, $P < 0.01$. Scale bar: 20 µm.

Supplementary Figure 5. Mechanical force-induced translocation of zyxin requires TRPV4 and Rho signaling. Averaged data of total zyxin immunofluorescence labeling in Figure 9. One hour stretch increases particulum sizes of zyxin, which suggesting its translocation into stress fibers. This stretch-induced translocation of zyxin is inhibited by HC-06 and Y-27632. (N = 3); *, $P < 0.05$.

Supplementary Figure 6. TM cells express standard phenotype and focal adhesion markers. PCR. (A) Transcripts encoding MYOC, TIMP3, AQP1, MGP and ACTA2 are prominently expressed, together with RhoA, FAK, zyxin, vinculin and paxillin mRNAs; *Gapdh* and □-*tubulin*, loading controls. (B) Western blot with an anti-myocilin antibody. 2 day exposure of hTM cultures to 100 nM DEX upregulated myocilin expression (N = 2). (C) Immunolabeling for anti-myocilin antibody after 2 day exposure to 100 nM DEX treatment, showing positive signals in TM cells (N = 2). Scale bar: 50 µm.

Supplementary Figure 7. TRPV4 and Rho-signaling modulate stretch-induced cytoskeletal reorganization in primary cells. Western blots of representative marker and cytoskeletal proteins in primary TM cells. (A) Raw data. (B - E) Averaged results (N = 2). Stretch-evoked expression and the effects of HC-06 and Y-27632 -in primary TM cells correspond to the effects seen in immortalized cells. Myocilin expression, however, is unaffected by stretch.

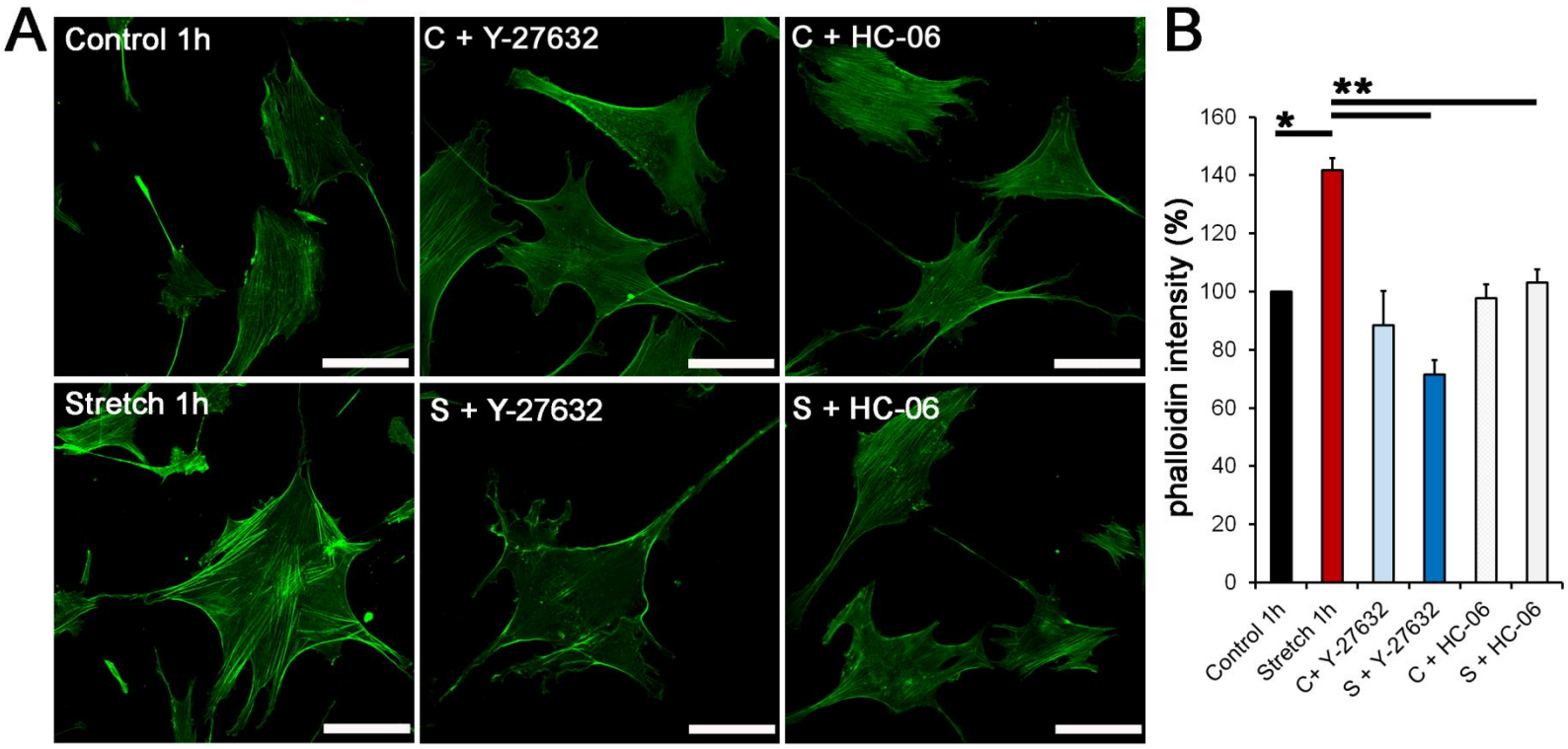
A
Control 1h
C + Y-27632
C + HC-06
Stretch 1h
S + Y-27632
S + HC-06
B
phalloidin intensity (%)
160
140
120
100
80
60
40
20
0
*
**
Control 1h
Stretch 1h
C+ Y-27632
S + Y-27632
C + HC-06
S + HC-06

Fig. 1

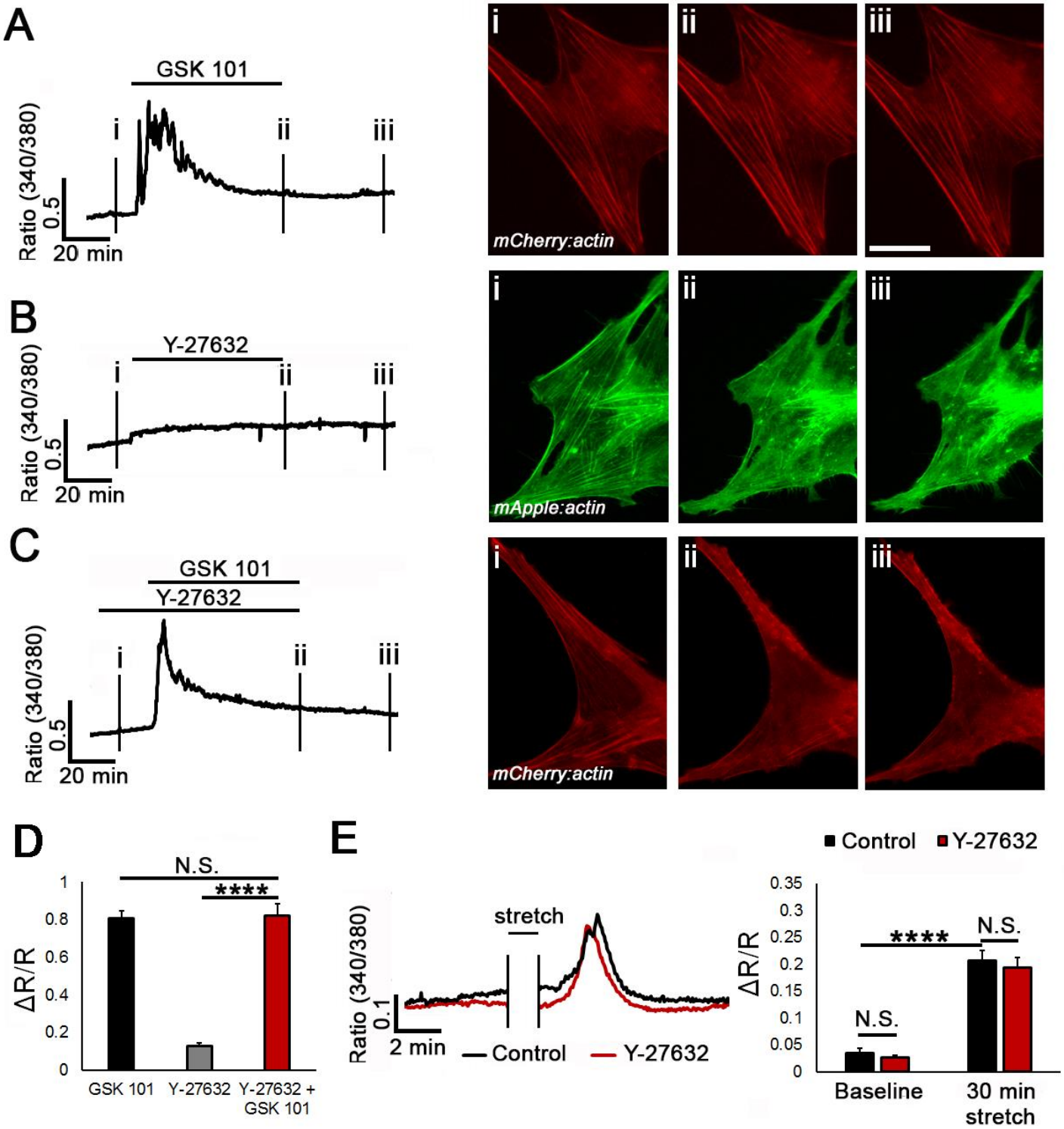
A
GSK 101
i
ii
iii
Ratio (340/380)
0.5
20 min
mCherry:actin
B
Y-27632
mApple:actin
C
GSK 101
Y-27632
mCherry:actin
D
N.S.
****
ΔR/R
1
0.8
0.6
0.4
0.2
0
GSK 101
Y-27632
Y-27632 + GSK 101
E
stretch
Ratio (340/380)
0.1
2 min
Control
Y-27632
0.35
0.3
0.25
0.2
0.15
0.1
0.05
Baseline
30 min stretch

Fig. 2

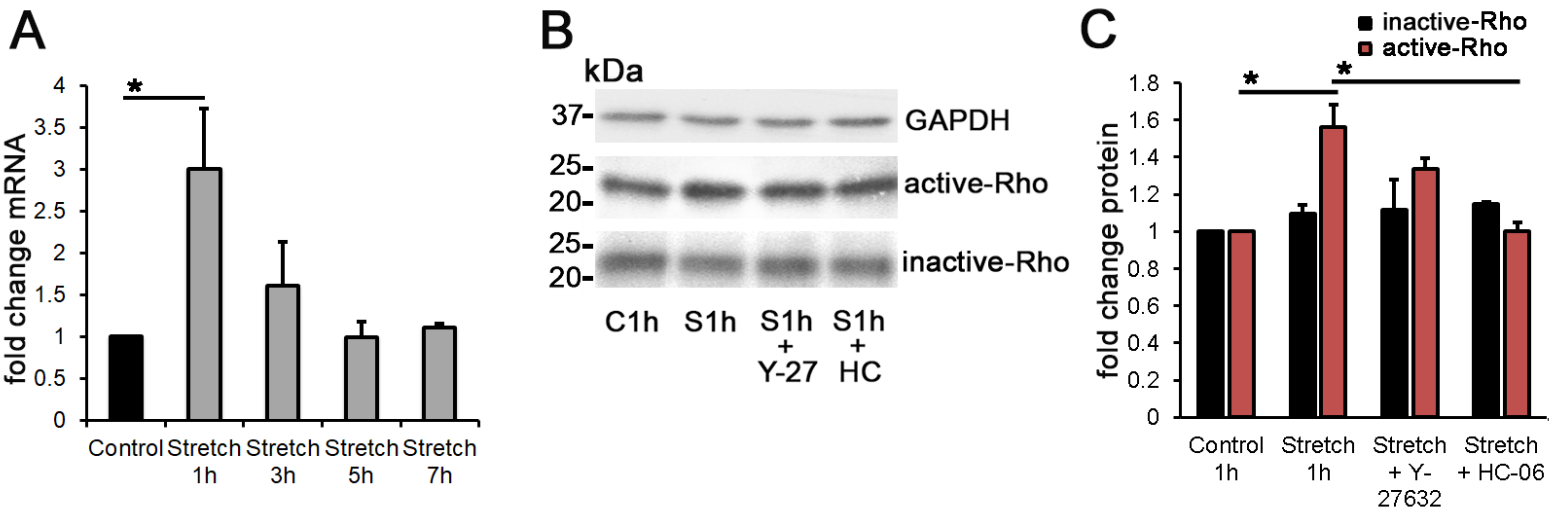
A
fold change mRNA
4
3.5
3
2.5
2
1.5
1
0.5
0
*
Control
Stretch 1h
Stretch 3h
Stretch 5h
Stretch 7h
B
kDa
37-
25-
20-
25-
20-
GAPDH
active-Rho
inactive-Rho
C1h
S1h
S1h + Y-27
S1h + HC
C
inactive-Rho
active-Rho
fold change protein
1.8
1.6
1.4
1.2
1
0.8
0.6
0.4
0.2
0
*
*
Control 1h
Stretch 1h
Stretch + Y-27632
Stretch + HC-06

Fig.3

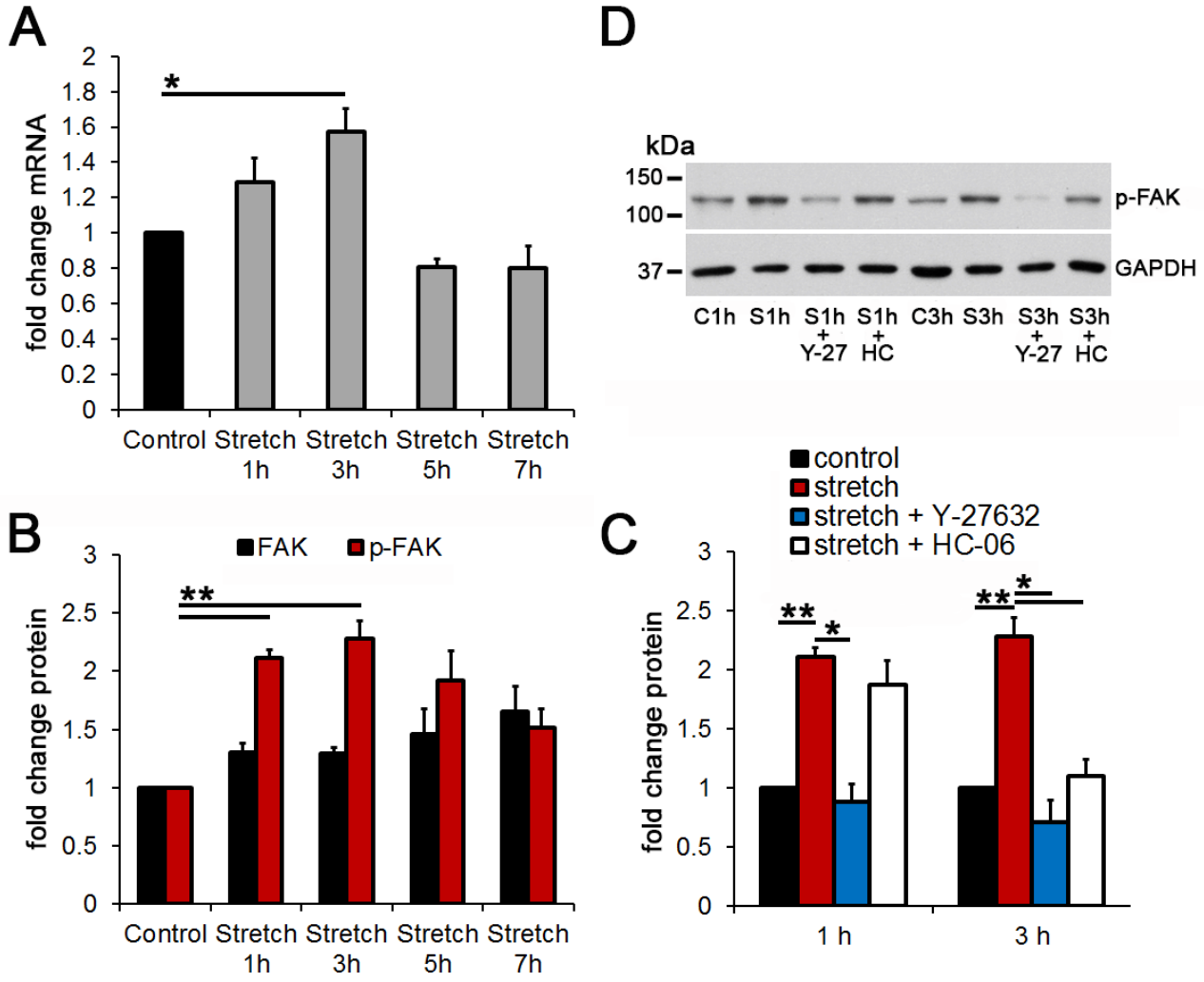
A
fold change mRNA
2
1.8
1.6
1.4
1.2
1
0.8
0.6
0.4
0.2
0
*
Control
Stretch 1h
Stretch 3h
Stretch 5h
Stretch 7h
D
kDa
150
100
37
p-FAK
GAPDH
C1h
S1h
S1h + Y-27
S1h + HC
C3h
S3h
S3h + Y-27
S3h + HC
B
FAK
p-FAK
fold change protein
3
2.5
2
1.5
1
0.5
0
**
Control
Stretch 1h
Stretch 3h
Stretch 5h
Stretch 7h
C
control
stretch
stretch + Y-27632
stretch + HC-06
fold change protein
3
2.5
2
1.5
1
0.5
0
**
*
**
*
1 h
3 h

Fig. 4

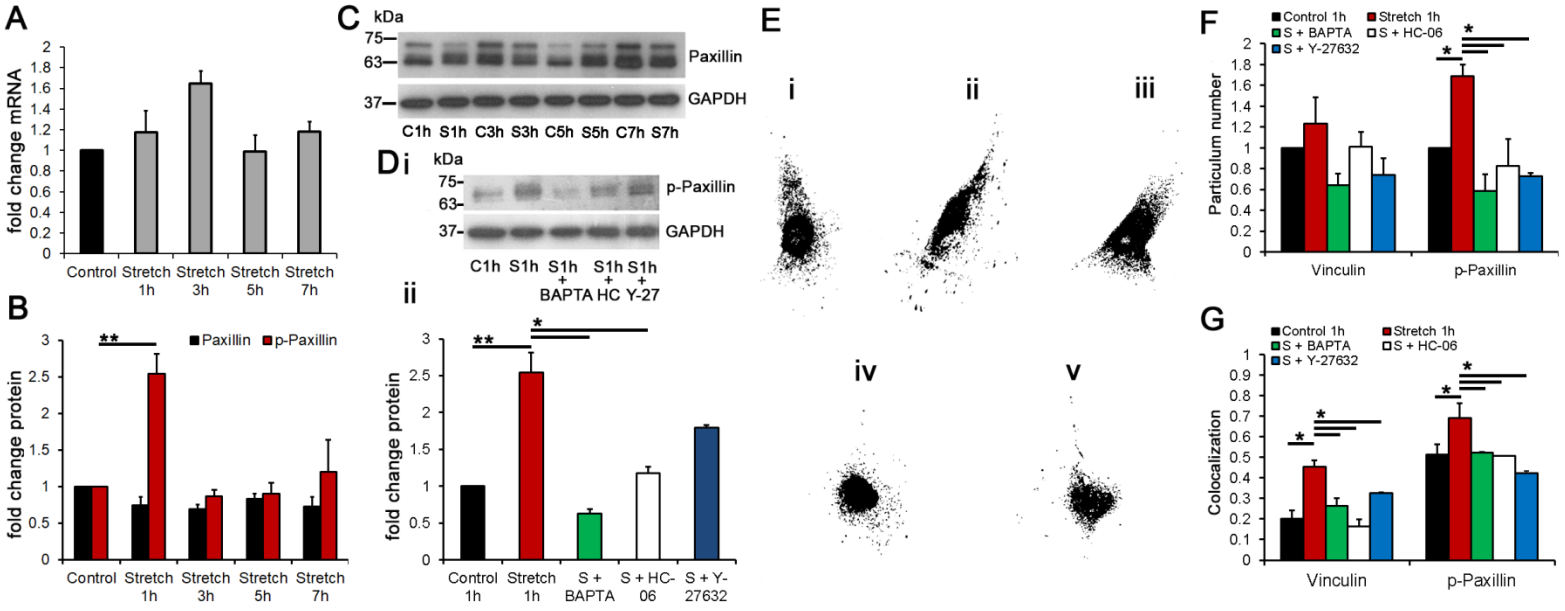
A
fold change mRNA
Control
Stretch 1h
Stretch 3h
Stretch 5h
Stretch 7h
B
fold change protein
Paxillin
p-Paxillin
C
kDa
75
63
37
Paxillin
GAPDH
C1h S1h C3h S3h C5h S5h C7h S7h
D i
p-Paxillin
GAPDH
C1h S1h S1h + BAPTA S1h + HC S1h + Y-27
ii
Control 1h
Stretch 1h
S + BAPTA
S + HC-06
S + Y-27632
E
i
ii
iii
iv
v
F
Control 1h
Stretch 1h
S + BAPTA
S + HC-06
S + Y-27632
Particulum number
Vinculin
p-Paxillin
G
Colocalization
Vinculin
p-Paxillin

Fig. 5

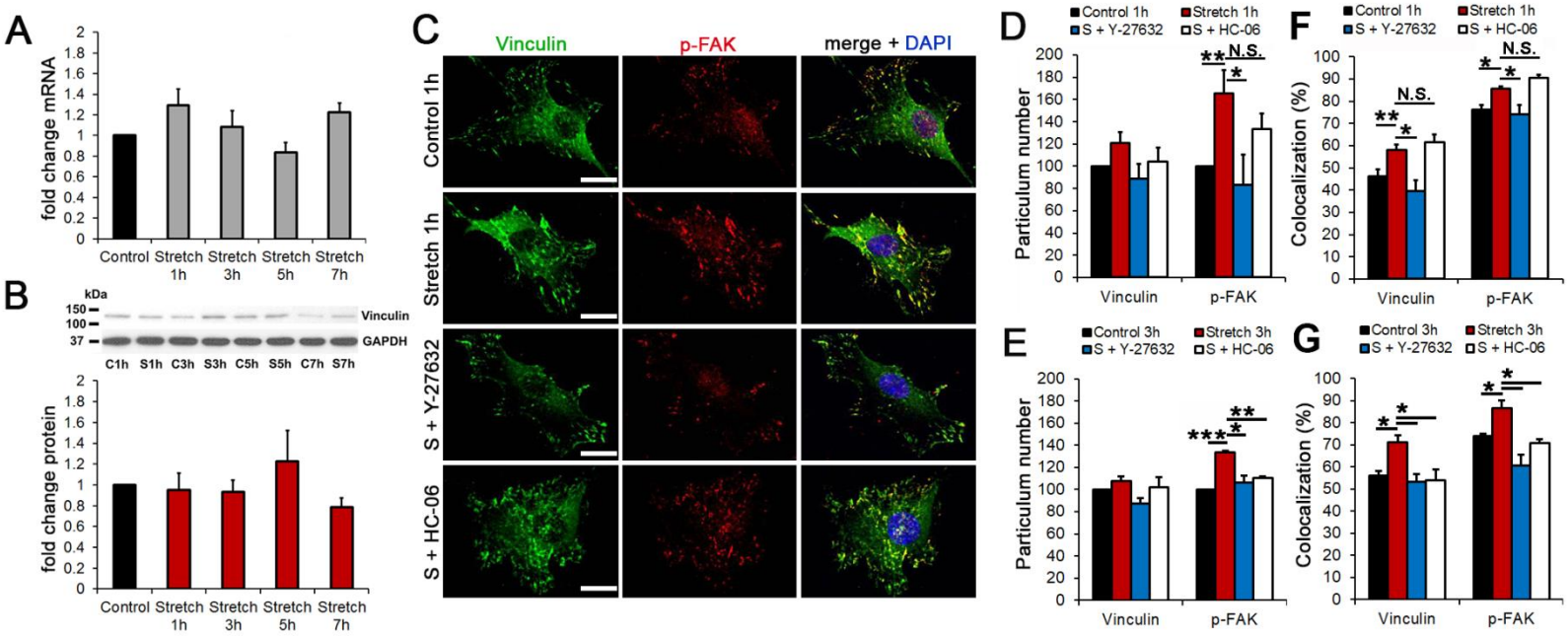
A
fold change mRNA
Control
Stretch 1h
Stretch 3h
Stretch 5h
Stretch 7h
B
kDa
150
100
37
Vinculin
GAPDH
C1h S1h C3h S3h C5h S5h C7h S7h
fold change protein
C
Vinculin
p-FAK
merge + DAPI
Control 1h
Stretch 1h
S + Y-27632
S + HC-06
D
Control 1h
Stretch 1h
S + Y-27632
S + HC-06
Particulum number
N.S.
E
Control 3h
Stretch 3h
S + Y-27632
S + HC-06
F
Colocalization (%)
G

Fig. 6

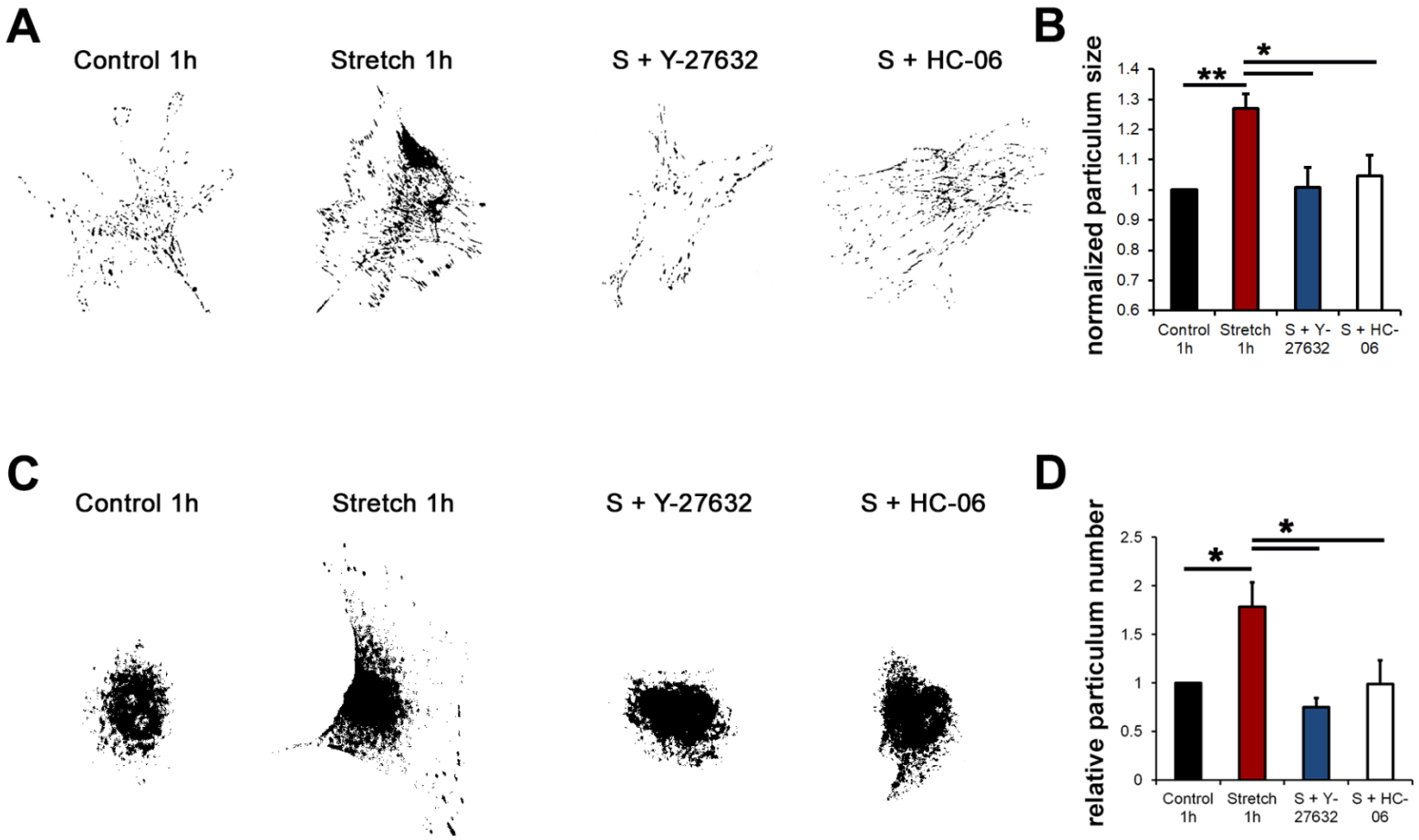
A
Control 1h
Stretch 1h
S + Y-27632
S + HC-06
B
normalized particulum size
1.4
1.3
1.2
1.1
1
0.9
0.8
0.7
0.6
**
*
Control 1h
Stretch 1h
S + Y-27632
S + HC-06
C
Control 1h
Stretch 1h
S + Y-27632
S + HC-06
D
relative particulum number
2.5
2
1.5
1
0.5
0
*
*
Control 1h
Stretch 1h
S + Y-27632
S + HC-06

Fig. 7

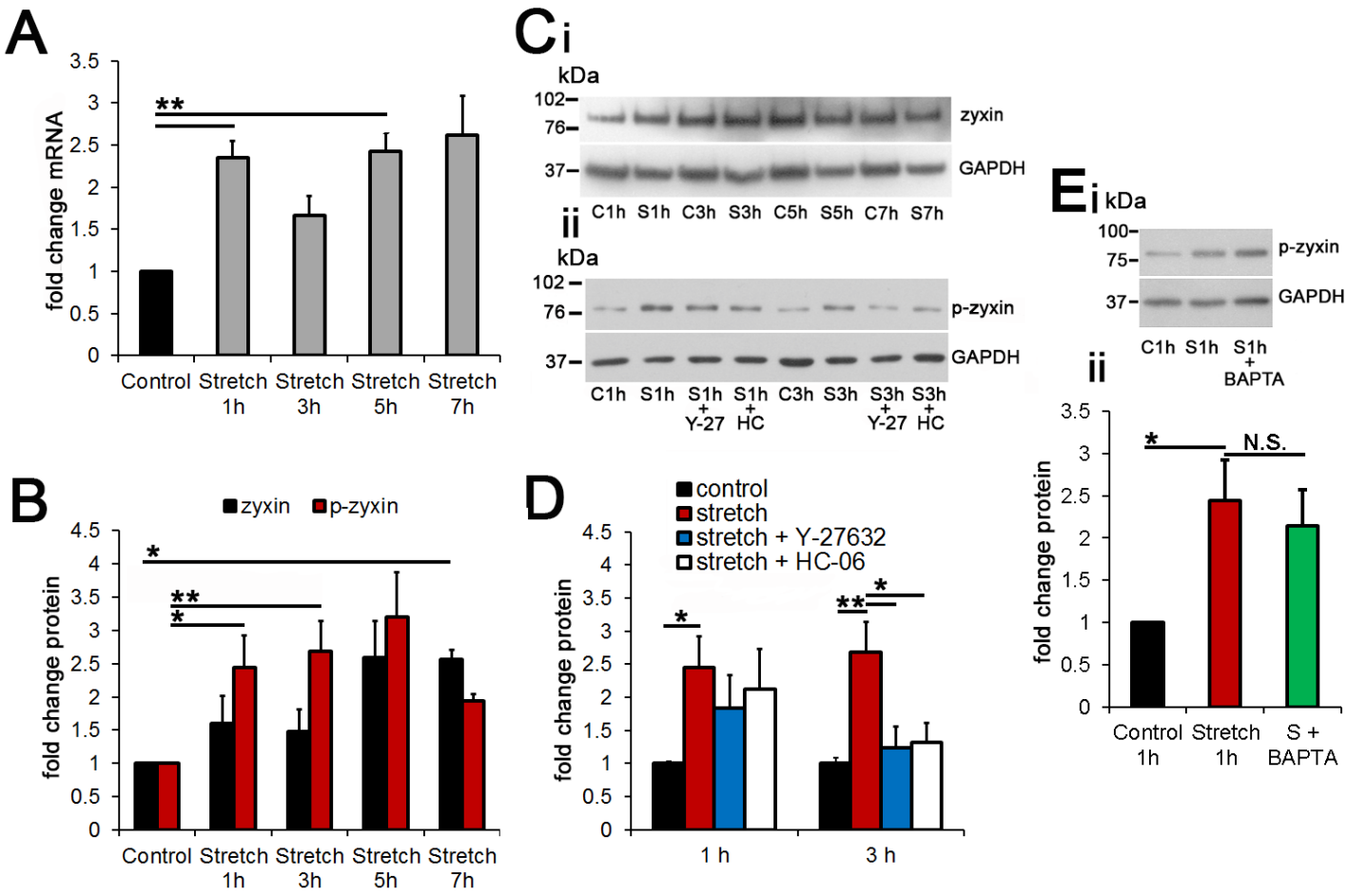
A
fold change mRNA
Control
Stretch 1h
Stretch 3h
Stretch 5h
Stretch 7h
Ci
kDa
zyxin
GAPDH
C1h S1h C3h S3h C5h S5h C7h S7h
ii
p-zyxin
C1h S1h S1h + Y-27 S1h + HC C3h S3h S3h + Y-27 S3h + HC
Ei
p-zyxin
C1h S1h S1h + BAPTA
N.S.
fold change protein
S + BAPTA
B
zyxin
p-zyxin
D
control
stretch
stretch + Y-27632
stretch + HC-06
1 h
3 h

Fig. 8

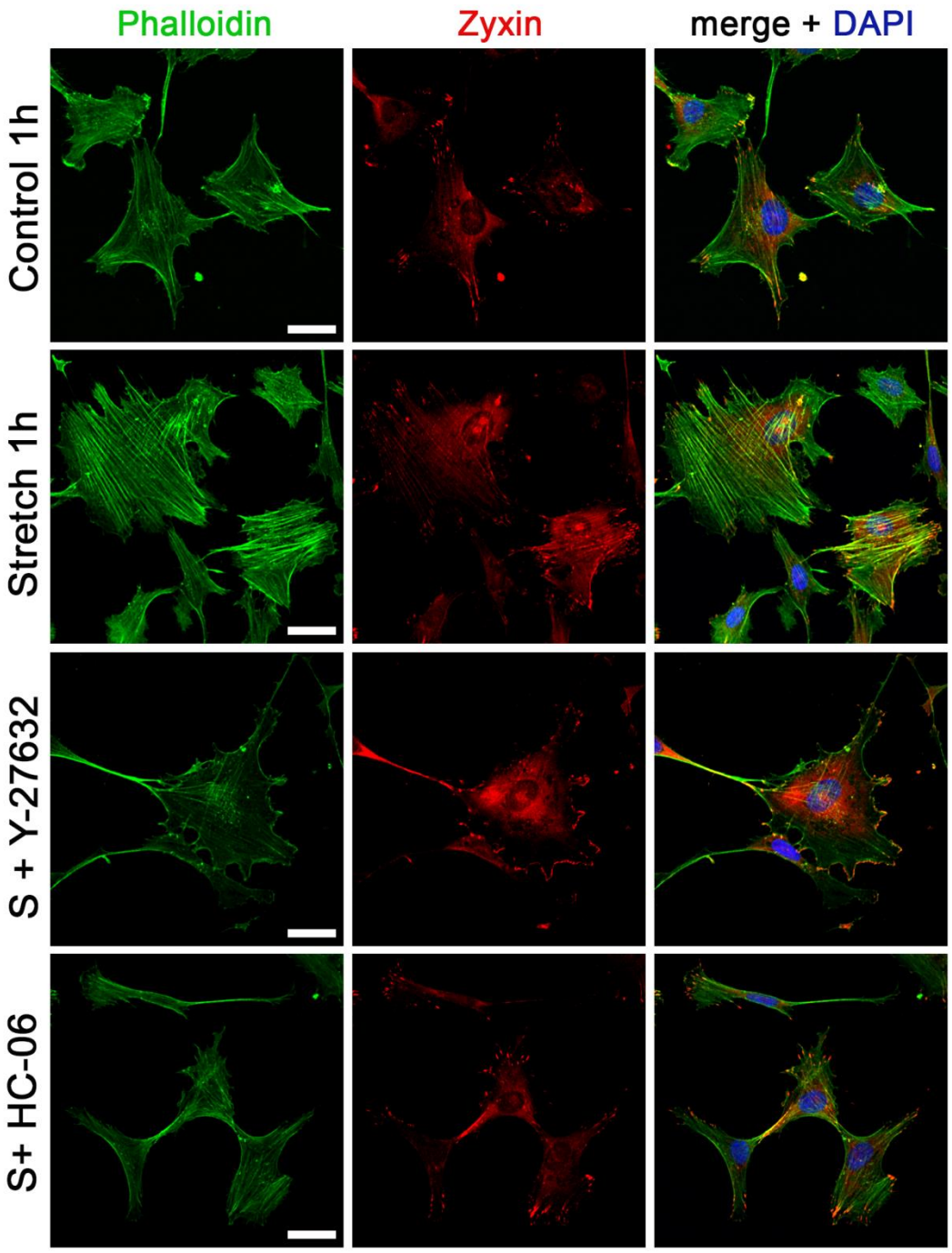
Phalloidin
Zyxin
merge + DAPI
Control 1h
Stretch 1h
S + Y-27632
S+ HC-06

Fig. 9